MEMBER BUCKLING IN USFOS

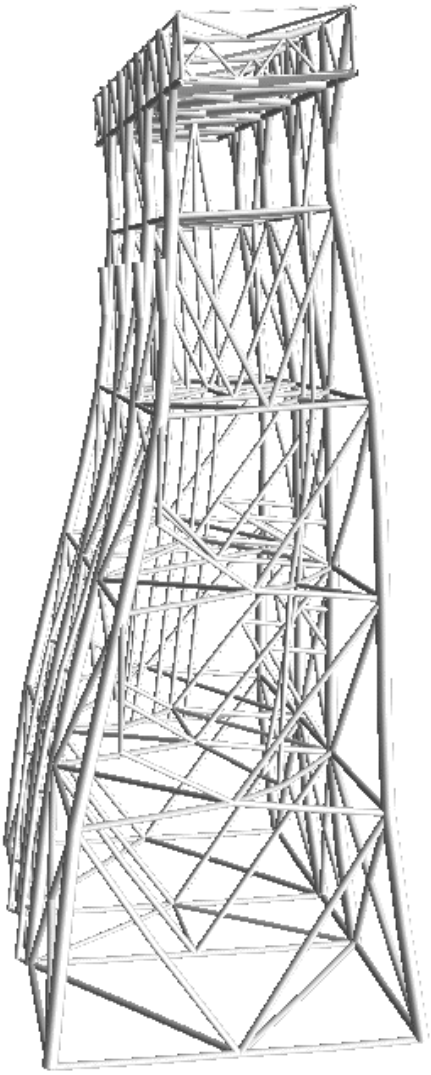

CONTENTS:

1 Introduction

1.1 Why must imperfections be introduced?

Real structures have imperfections, notably in the form of out–of-straightness and residual stresses, both on local and systems level. Residual stresses and imperfections are mutually dependent. The magnitude and direction of imperfections generally not well known.

For members of a structural system to buckle, lateral displacement of member mid-section has to be present, either as ***initial imperfections or imposed by frame deformations in pre-buckled state***. Lateral displacement must be > ***~10^{-5} member length*** in order to provoke buckling.

In some cases pre-buckling lateral displacements are not sufficient, and buckling resistance ***is either overestimated or numerical problems are encountered***. This is avoided by introducing initial imperfections in the system.

The imperfections should be selected such ***that inherent conservatism in the characteristic column buckling curves from Design codes is preserved***. In this way the nonlinear analysis reflects additional strength due to the redundancy of the system.

Characteristic column buckling curves, which contain the effect of true imperfections and residual stresses), are often simulated very well by means of an ***equivalent imperfection***. Very often this imperfection is approximately equal to the tolerance level for out-of-straightness specified by the code. (In fact, Eurocode 3 column curves are based upon the concept of equivalent imperfection)

1.2 In what direction shall imperfections be applied?

The true directions are not known. They depend on the fabrication processes from the steel mills to platform construction. The directions are more or less of random nature.

When the true directions are not known we must be conservative and select directions that have the largest impact on the buckling resistance.

O. Hellan (1995) investigated a few alternatives:

- Lowest eigenvector of system stiffness matrix
- Displacement vector at system collapse
- Elastic system buckling mode
- Linear solution vector of the external load
- Global base shear (resultant load)
- The (distributed) loading of the individual members

Pushover analyses of several typical North Sea jackets were carried all the above alternative. Figure 1-11-11-1 Shows normalised first member failure and system collapse histograms obtained by the analyses for imperfections in direction of global base shear.

Figure 1-21-21-2 shows the normalised first member failure and system collapse with respect to mean value and standard deviation for different imperfection patterns.

It is observed that applying the imperfections in the direction of applied member load or global base shear, consistently gives the smallest mean values and a small standard deviation. Hellan concluded therefore, that these directions should be used.

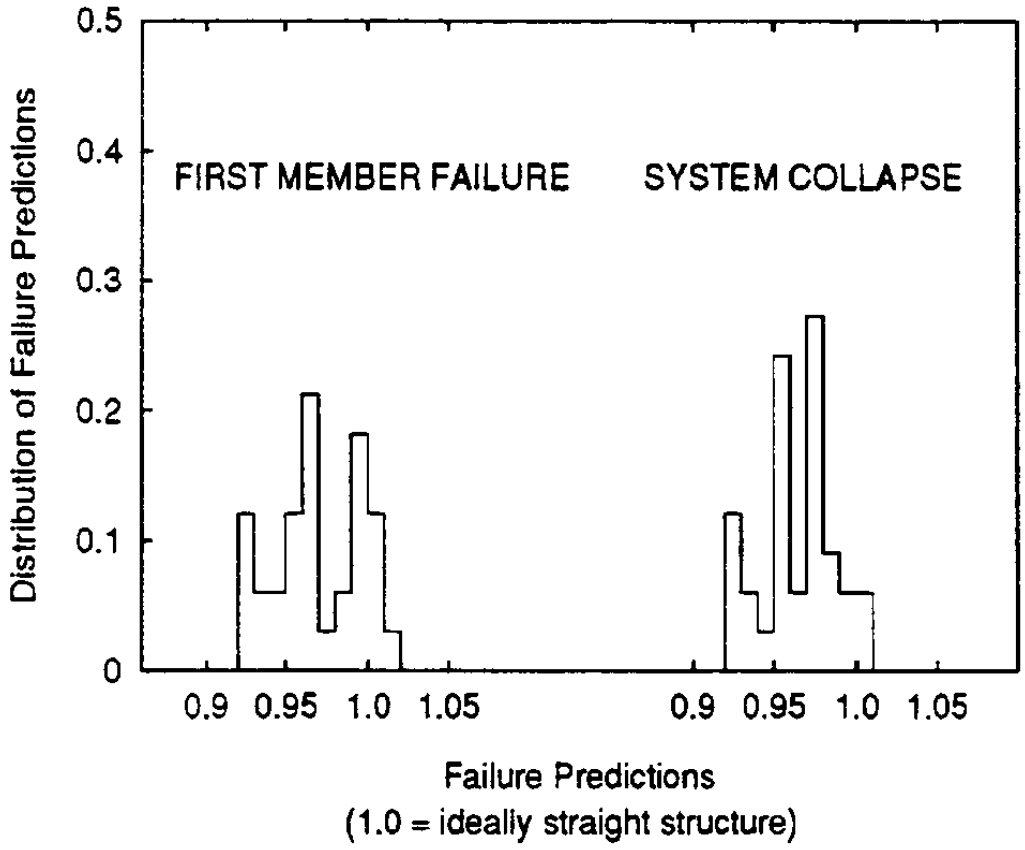

Figure 1-1 Normalised first member failure and system collapse. Histogram for imperfections in direction of global base shear,

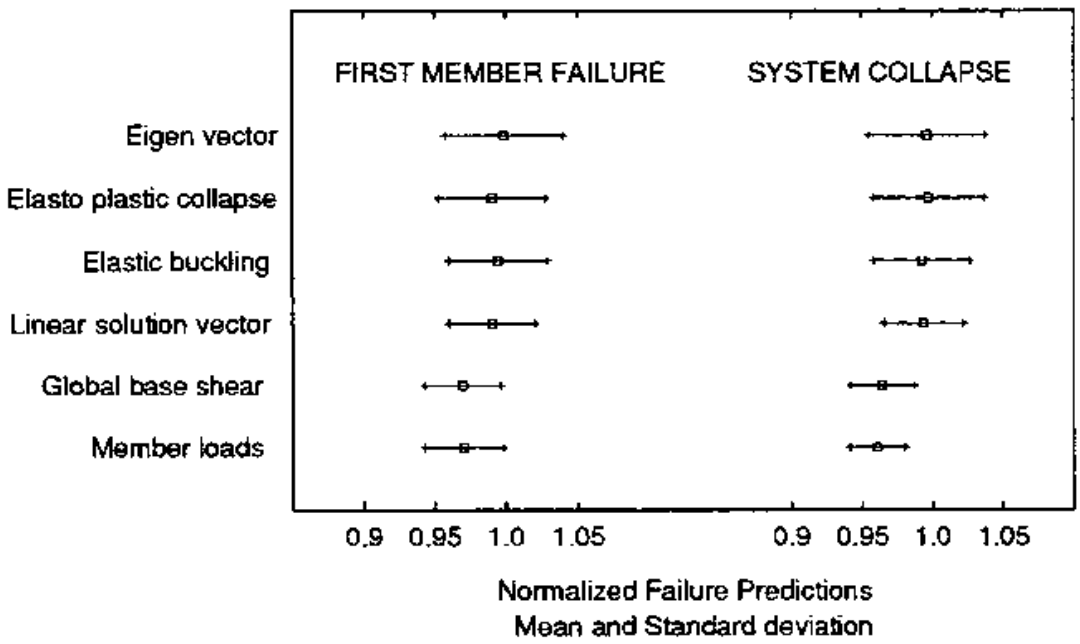

Figure 1-2 Normalised first member failure and system collapse. Mean value and standard deviation for different imperfection patterns (Figure 5.4 in *Nonlinear Pushover and Cyclic Analysis in Ultimate Limit State Design and reassessment of Tubular Steel Offshore Structures*, PhD Thesis by Øvind Hellan, 1995)

1.3 USFOS – strategy for application of imperfections

- Imperfection in direction of applied load or global base shear
- Magnitude according to tolerance requirements in codes (typically ~ l/1000)
- Automatic calibration to various design codes offered
  - API_WSD
  - API_LRFD
  - ISO19902
  - NORSOK N-004
- The calibration is based on code column ***characteristic values***, i.e. the partial safety factor for the resistance is NOT included.
- The resistance safety factors for ULS type of analyses should be applied on the load side, defining a target load equal to the action factor times the resistance factor.
- API_WSD defines a maximum utilization of 0.60 with respect to column buckling. This factor is included in the calibration, i.e. the basic column curve is multiplied with 5/3.
- Interaction between local buckling and column buckling is automatically included in USFOS when the dent formulation is active. Local buckling is treated as an increased imperfection

- NORSOK contains a shell slenderness dependent partial safety factor for the resistance that accounts for possible interaction between local axial failure and hoop buckling of members subjected to axial compression and bending and hydrostatic pressure. This factor must be considered on the load side.

The Perry-Robertson approach is used to get the correct column buckling stress according to a given code. This is obtained by scaling an initial imperfection, w_0, such that failure occur for an axial stress $f = f_c$, where f_c is the characteristic column buckling stress for a given slenderness:

$$\frac{f_c}{f_{cl}} + \frac{f_c A w_0}{W f_{cl}} \frac{1}{1 - \frac{f_c}{f_E}} = 1$$

f_{cl} is the characteristic yield strength or the characteristic stress for local buckling for axial compression. f_E is the Euler buckling stress. This yields the following amplitude for the imperfection

$$w_0 = \frac{W}{A}\left(\frac{f_{cl}}{f_c} - 1\right)\left(1 - \frac{f_c}{f_E}\right).$$

Modiufication for local buckling

According to ISO 19902/NORSOKthe characteristic local buckling resistance is determined given as :

$$\frac{f_{cl}}{f_y} = 1.0 \qquad \bar{\lambda} \le 0.412$$

$$\frac{f_{cl}}{f_y} = 1.047 - 0.274\bar{\lambda}^2 \qquad 0.412 \le \bar{\lambda} \le 1.382$$

$$f_{cl} = f_{ce} \qquad 1.382 \le \bar{\lambda}$$

in which $\bar{\lambda} = \sqrt{\frac{f_{xe}}{f_y}}$ and $f_{cle} = C_x E \frac{t}{r}$

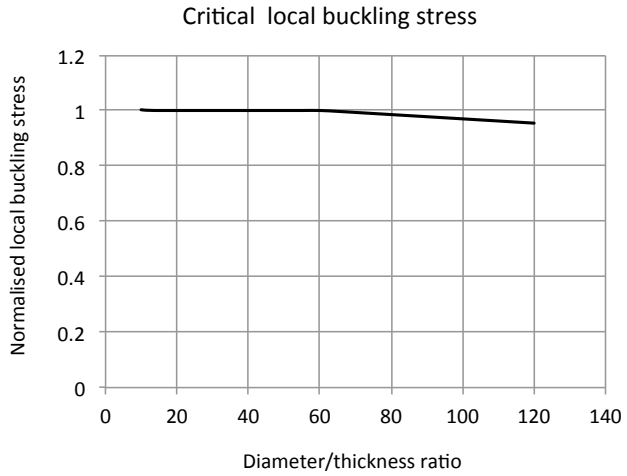

Figure 1-3 Local buckling strength versus D/t-ratio. Fy = 355 Mpa

It is seen that the reduction in capacity due to local buckling increases moderately for D/t > 60. It is very impractical to have two "yield" strength factors, f_y and f_{cl} in USFOS. Alternatively, the yield strength f_y is used regardless of the diameter/thickness ratio, and the correct column buckling strength, f_c, is obtained by scaling up the initial imperfection.

Effect of hydrostatic pressure

Hydrostatic pressure causes a hoop stress $\sigma_h = pr/t$ and axial stress $\sigma_x = pr/2t$ in closed cylinders. This presence of these stresses reduces the stress available for elasto-plastic column buckling. The column buckling stress, f_{ch}, which accounts for the effect of hydrostatic pressure is calculated through the following interaction equation:

$$\left(\frac{f_{ch}}{f_{cl}}\right)^2 - \left(\frac{f_c}{f_{cl}} - \frac{2\sigma_x}{f_{cl}}\right)\frac{f_{ch}}{f_{cl}} + \frac{\sigma_x}{f_{cl}}\left(\frac{\sigma_x}{f_{cl}} - 1\right) = 0, \quad \bar{\lambda} < 1.34\sqrt{\left[(1 - \frac{2\sigma_x}{f_{cl}})\right]^{-1}} \qquad (1.1)$$

where f_{cl} is the equivalent yield stress accounting for local buckling and f_c is the basic column buckling strength.
Solved with respect to f_{ch} this becomes:

$$\frac{f_{ch}}{f_{cl}} = \frac{1}{2}\left[\xi - \frac{2\sigma_x}{f_{cl}} + \sqrt{\xi^2 + 1.12\,\bar{\lambda}^2\frac{\sigma_x}{f_{cl}}}\right], \quad \bar{\lambda} < 1.34\sqrt{\left[(1 - \frac{2\sigma_x}{f_{cl}})\right]^{-1}} \qquad (1.2$$

where $\xi = 1 - 0.28\bar{\lambda}^2$. For reduced slenderness exceeding the above value there is no reduction due to hydrostatic pressure. In USFOS the effect of hydrostatic pressure is considered in the yield criterion. Hence, the same imperfection level is used regardless of the l hydrostatic pressure.

Partial safety factor

NORSOK specifies a partial safety factor for the resistance that depends on the shell slenderness parameter, λ_S

$$\gamma_M = 1.15 \qquad \bar{\lambda}_s < 0.5$$
$$\gamma_M = 0.85 + 0.60\bar{\lambda} \qquad 0.5 \le \bar{\lambda} \le 1.0$$
$$\gamma_M = 1.45 \qquad \bar{\lambda}_s > 1.0$$

Figure **1-41-4** Shows how the factor comes out to be for various water depths and diameter-thickness ratios. Small changes in the diameter/thickness ratio may have a big impact on the material factor

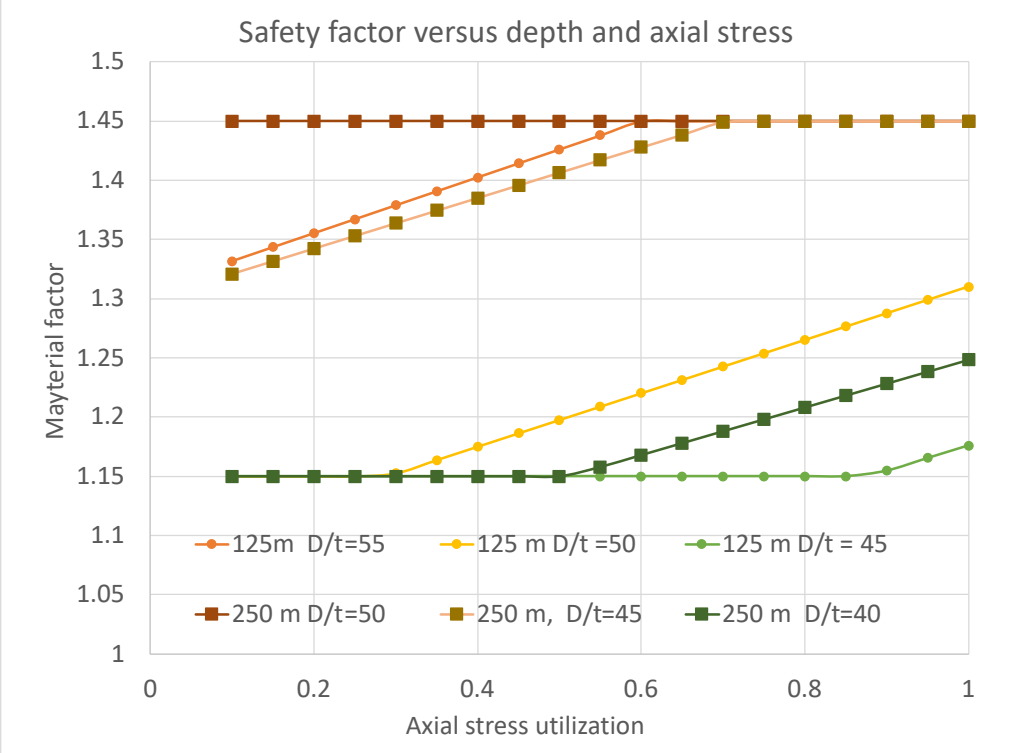

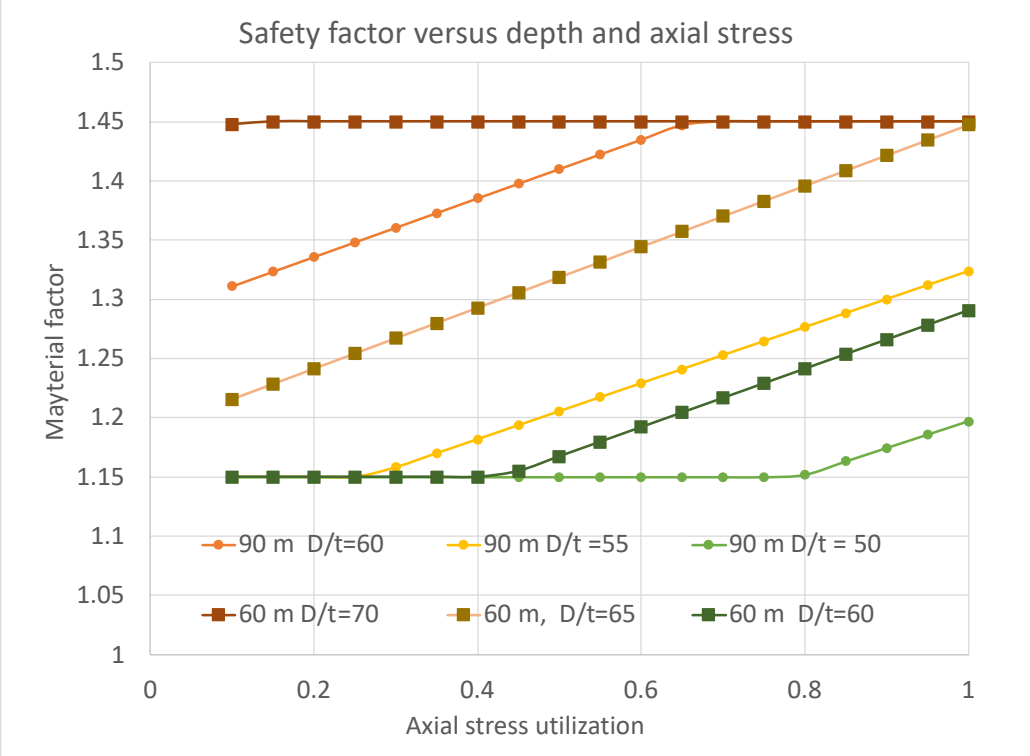

Figure 1-4 Material factor for various water depths and D/t-ratios. Yield stress f_y = 355 MPa, and hoop buckling based on "long" unstiffened tube *($\mu > 1.6D/t$)*

2 Simply supported Column

The two examples below shows that the calibration works well for both a single element and the same member subdivided into 10 elements. In the latter case, each sub-element gets the correct displaced nodes initial end rotations. For input description for the two examples, reference is made to Release Note for USFOS Version 8-6 (www.usfos.com/News)

2.1 Single element

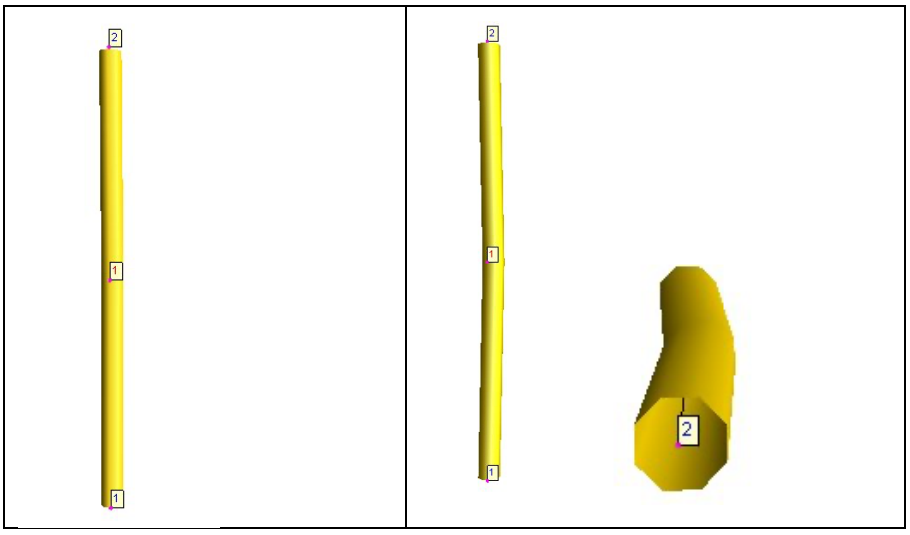

Figure 2-1 Initial deformations. API LRFD (left) and API WSD (right)

```
'
'            ColumnCurve   Pattern   LoadCase
 cIniDef       CURVE         Memb        1
'
```

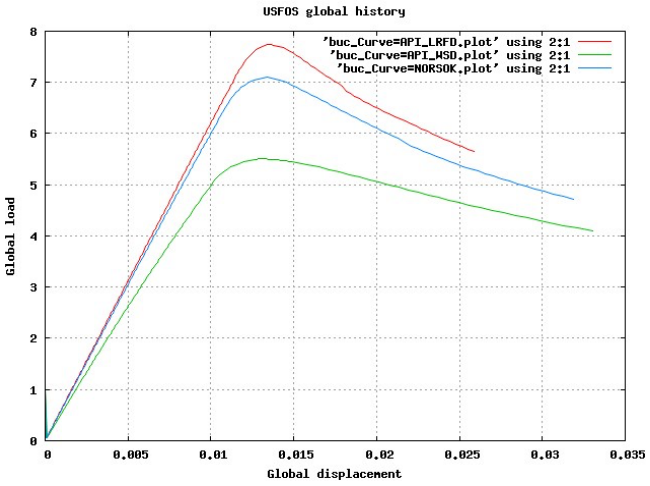

Figure 2-2 Global History for 3 different buckling curves.

2.2 Single Member, 10 elements

```
'
'            ColumnCurve  Pattern  LoadCase
 cIniDef       CURVE        Memb       1

'
'                     ImpGrp   ListTyp  Ids ....
 Member  Imperfect     Auto     Group     1
'
'
'              ID   ListTyp     Id ...
 GroupDef       1   Mat          1
```

Figure 2-3 USFOS commands. Defining member imperfection and element group

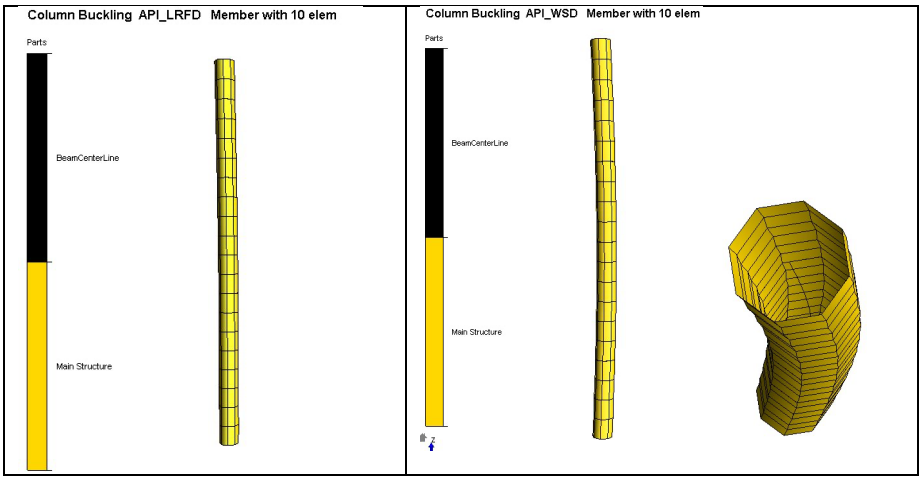

Figure 2-4 Initial deformations. API LRFD (left) and API WSD (right)

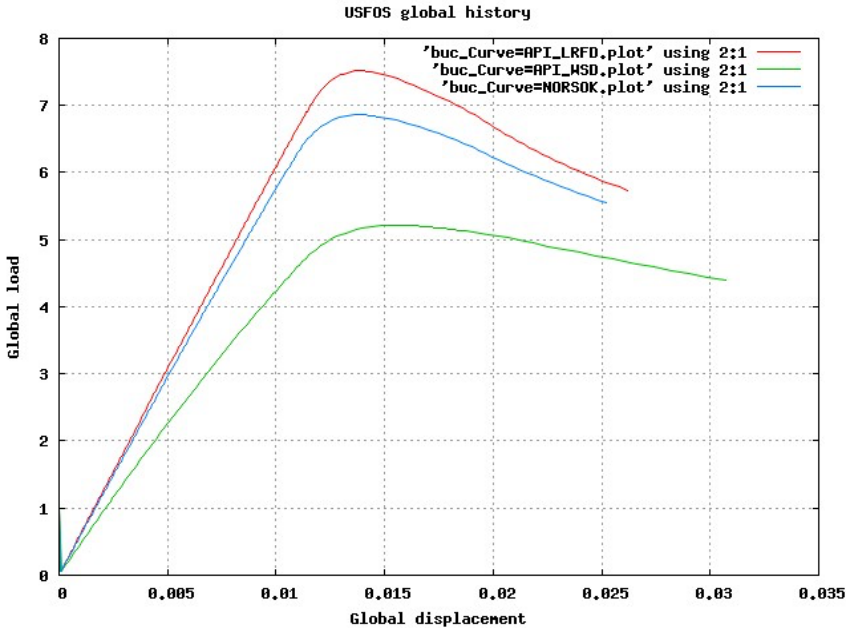

Figure 2-5 Global History for 3 different buckling curves.

3 Verification of the calibration to column curves

Figure 3-13-13-1 to Figure 3-83-83-7 show the results of the calibration to API WSD, API LRFD , ISO19902/NORSOK and ECCS/Eurocode column curves. It is emphasized that all analyses, except where noted, are carried out for default values of a = 0.25 for the elasto-plastic transition parameter. If non-default values are used, the agreement between USFOS results and the column curve is affected. (Generally, increasing “a” gives higher critical stress and vice verse).

The column curves are non-dimensional, but the imperfection levels reported depend on actual yield strength and the geometry. All calibrations are carried out for circular pipes with yield strength of 355 MPa.
The basic D/T-ratio is 50, but the influence of local buckling is checked for D/t = 100. The influence of hydrostatic pressure is also checked for D/t = 25.

3.1 API-WSD

The calibration to the API WSD curve is based the use of a safety factor 5/3 applied on the column curve given.Figure 3-13-13-1 shows results of the calibration to the column curve.

USFOS results match the column curve pretty swell, but are slightly conservative for intermediate column slenderness. The applied initial imperfection varies between 0.0015 and 0.0035 of the member length.

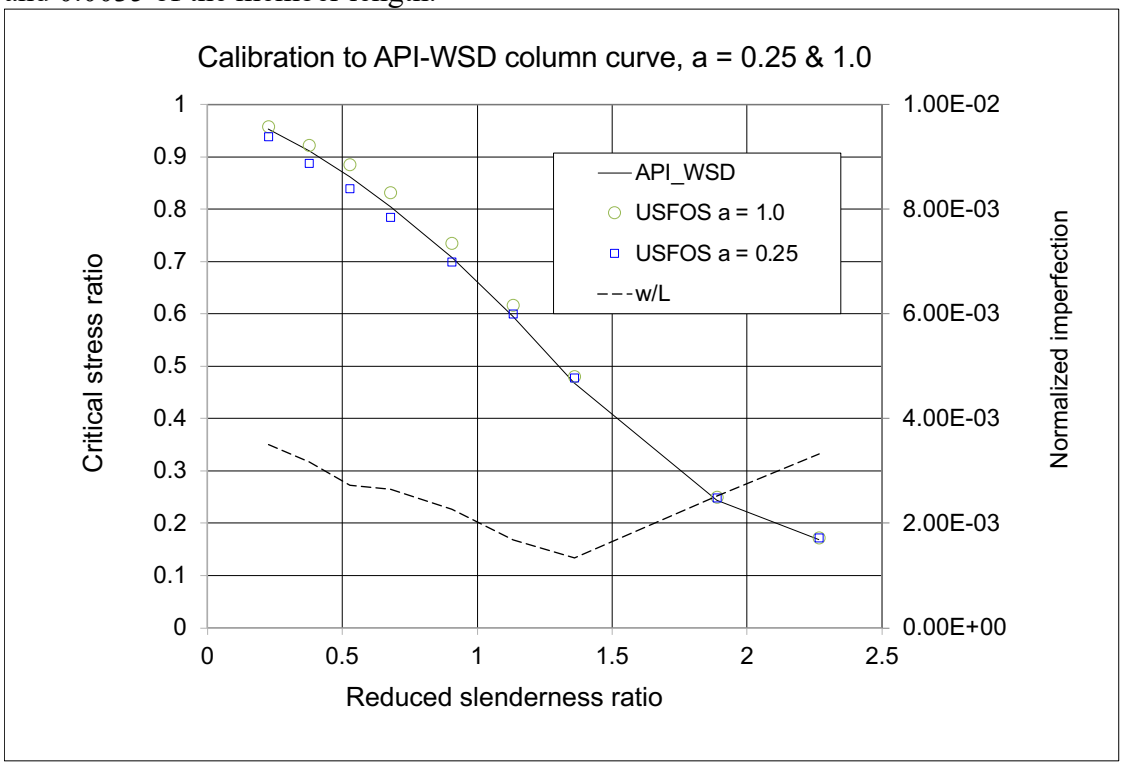

Figure 3-1 Calibration to API-WSD column curve, D/t = 50, a-factor = 0.25 (default) and 1.0

3.2 API-LRFD

Figure 3-23-23-2 shows calibration to API LRFD column curve. The agreement is good for the entire range of slendernesses. The imperfection level at maximum 0.001 (0.1%).

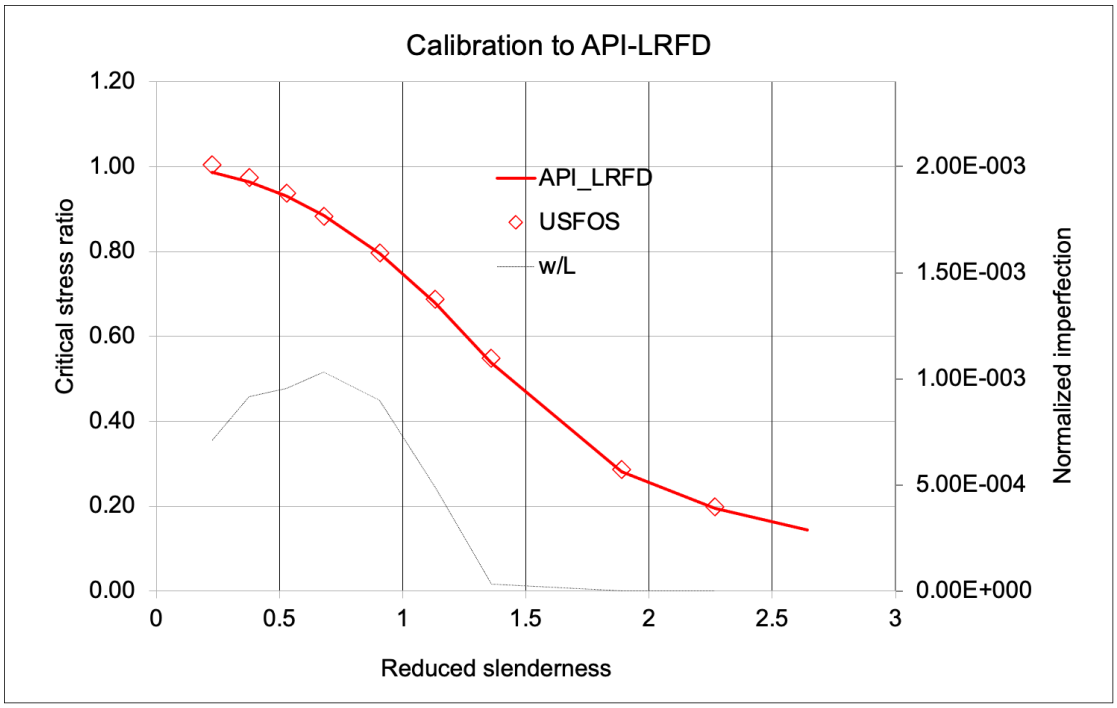

Figure 3-2 Calibration to API-LRFD column curve, a-factor = 0.25 (default)

3.3 ISO/NORSOK

For thin-walled members pre-ultimate local buckling may occur. In the ISO/NORSOK code this is taken into account by applying the local buckling strength as the effective yield strength in the column buckling check. The calibration is based on the same concept, and the use of reduced yield strength for thin-walled members in the calibration manifests itself as an increased imperfection for stocky columns as shown for D/t = 100.

Figure 3-33-33-3 shows that the calibration gives USFOS predictions in good agreement with the column curve for D/t = 50 and 100, but they are somewhat conservative for stocky columns.

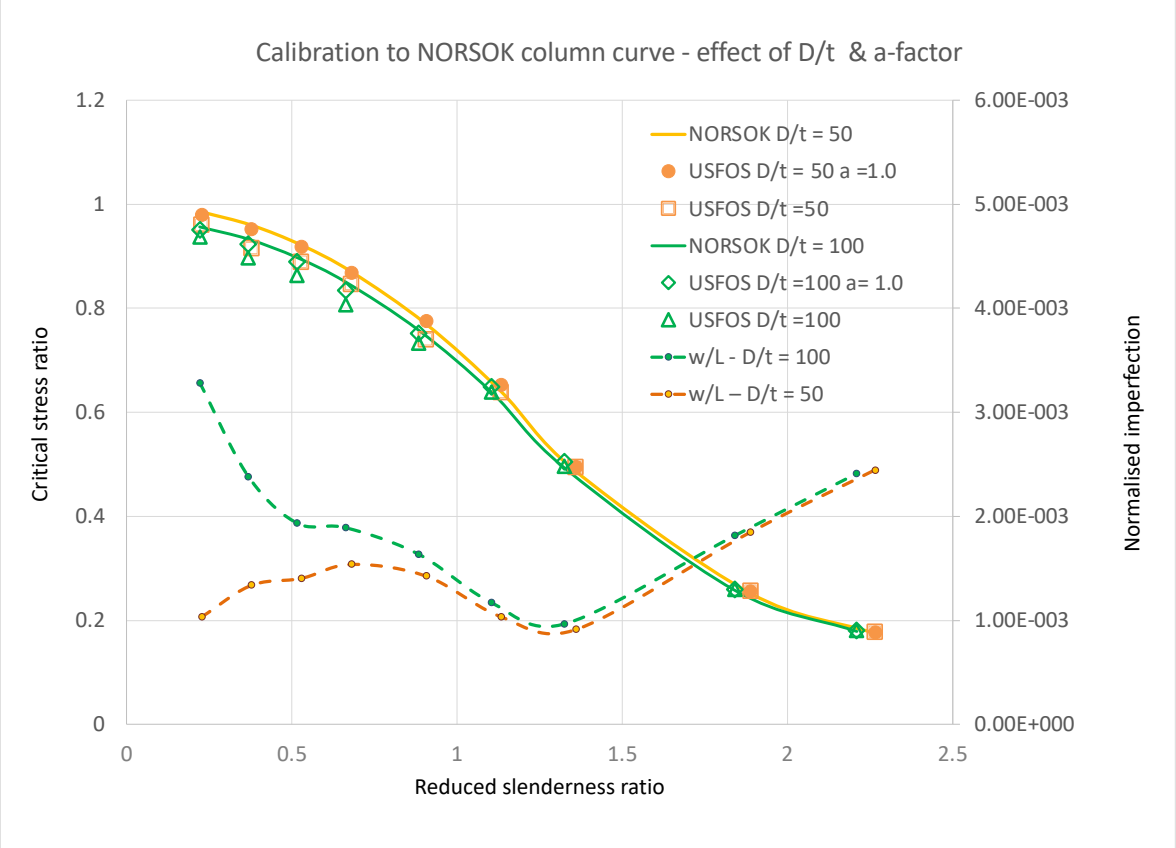

Figure 3-3 Calibration to NORSOK column curve with local buckling effect. D/t = 50 and100, a-factor = 0.25 (default) and 1.0

The imperfection level is in the range of 0.015 (1.5%) of member length for typical slenderness levels.

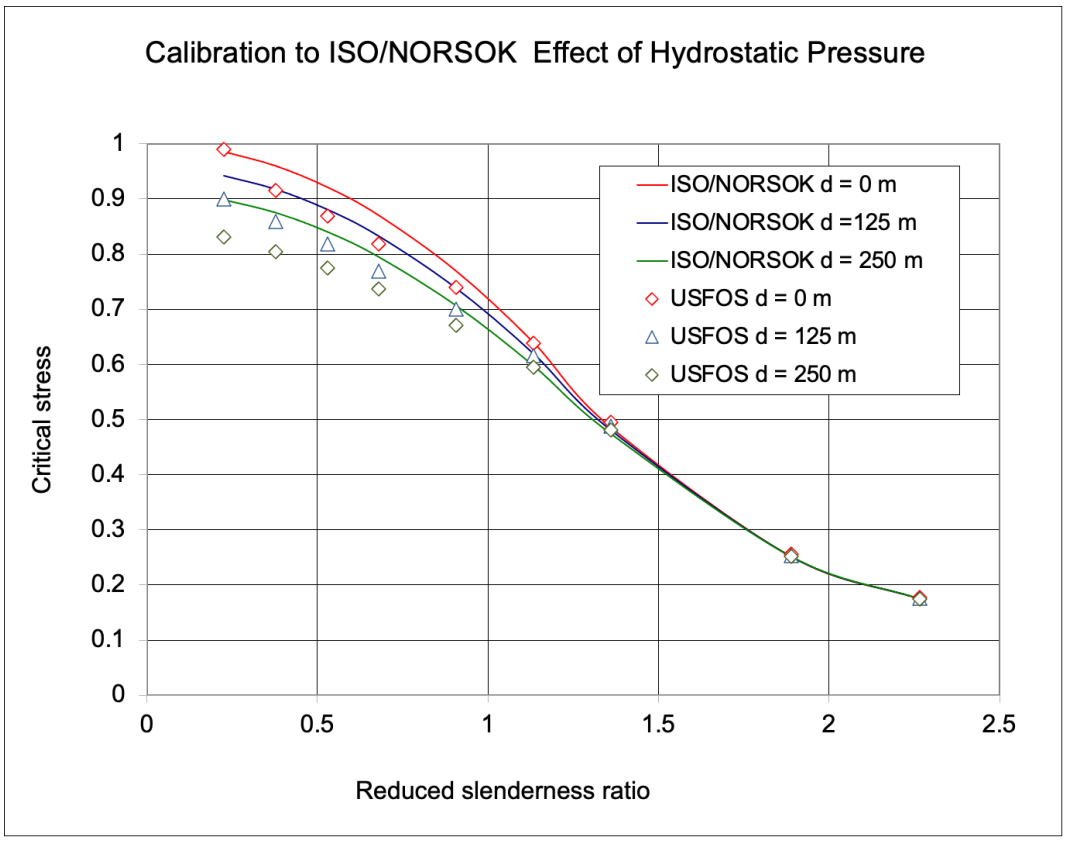

Figure 3-43-43-4 shows the effect of hydrostatic pressure on the ISO19902/NORSOK column curves for D/t = 50. The USFOS predictions are somewhat conservative for both 125 m and 250 m for stocky members, while slender members are little affected by hoop pressure. At 250 m depth, the D/t-ratio starts to become critical with respect to hoop buckling.

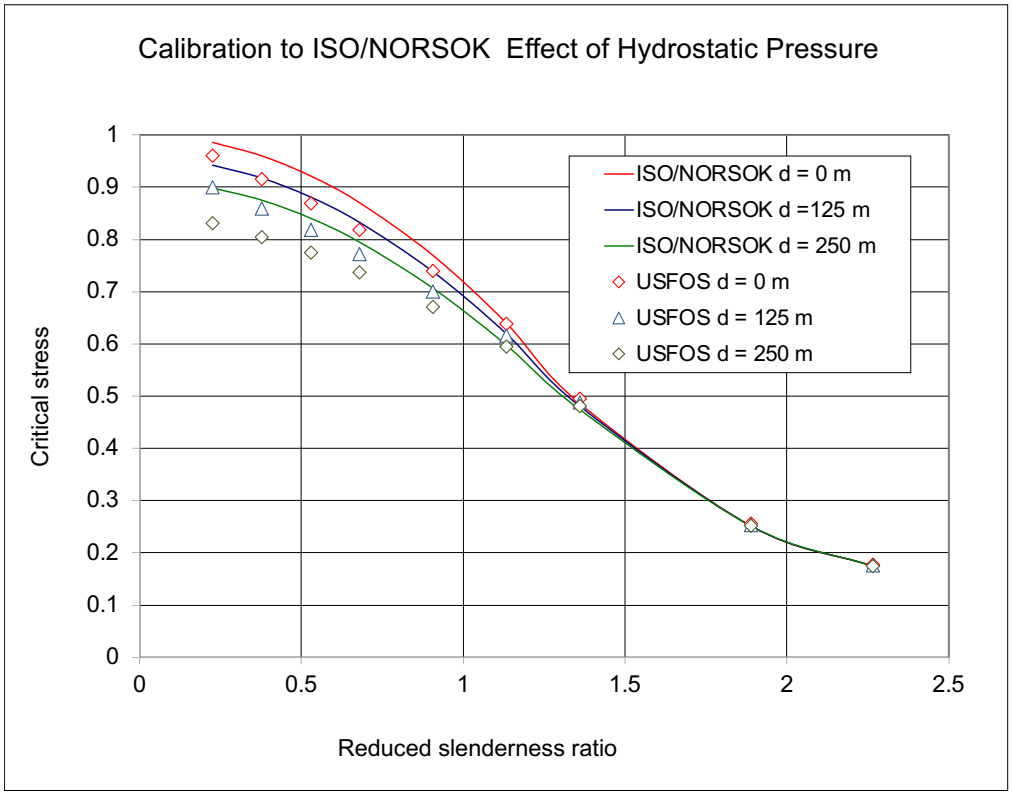

Figure 3-43-43-4 Calibration to ISO/NORSOK column curve with hydrostatic pressure D/t = 50, a-factor = 0.25 .

The effect of hydrostatic pressure is implicit in the USFOS beam model, through inclusion of hoop stresses in the yield criterion, and no additional imperfection is needed

The effect of local buckling /hydrostatic pressure is taken into account in the same manner also when the member is calibrated to API_LRFD and API_WSD column curves.

Figure 3-4 Calibration to ISO/NORSOK column curve with hydrostatic pressure D/t = 50, a-factor = 0.25 .

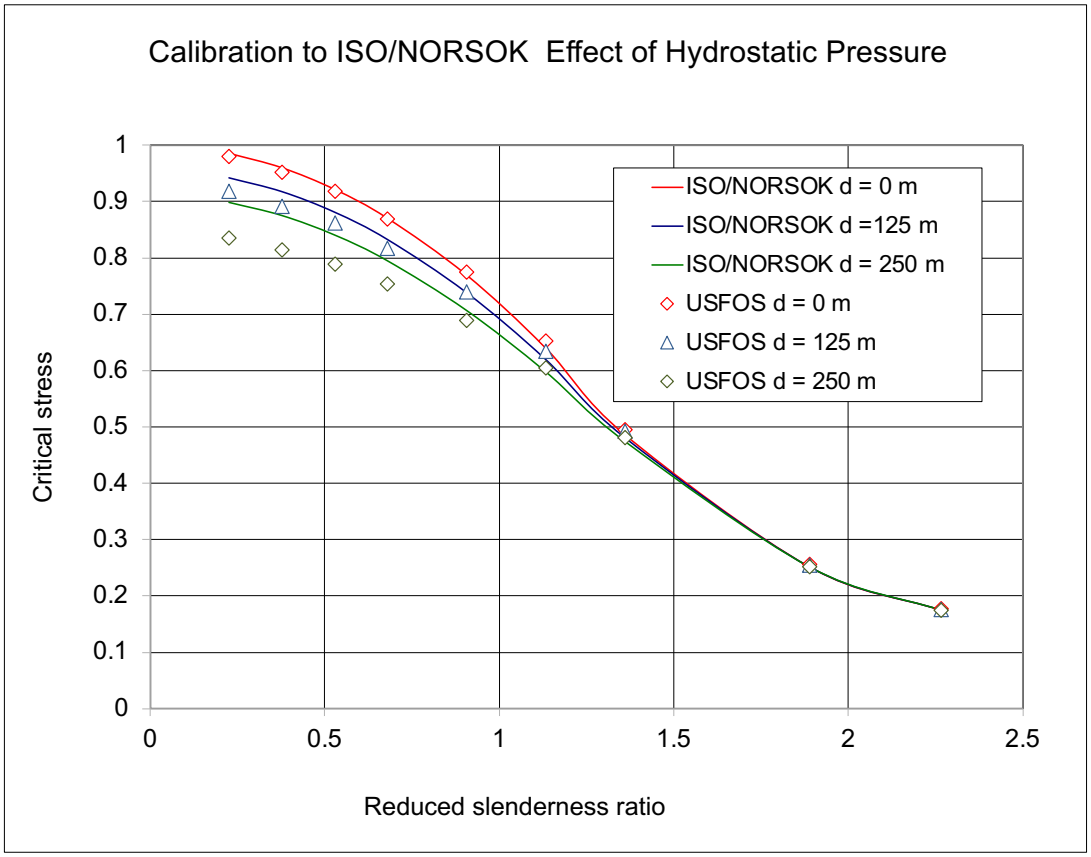

Figure 3-5 Calibration to ISO/NORSOK column curve with hydrostatic pressure D/t = 50, a-factor = 1.0

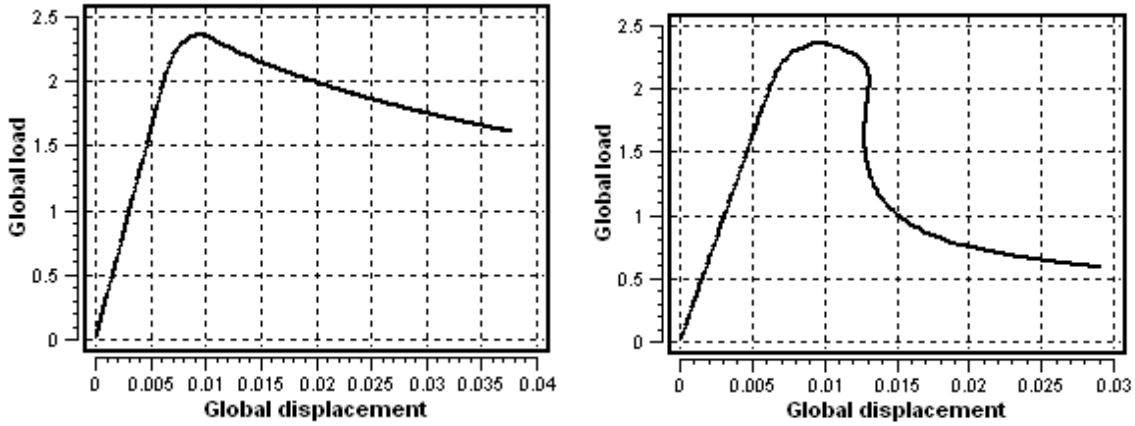

Figure 3-6 Buckling without local denting (left) and with dent (right)

3.4 ECCS/Eurocode 3

Figure 3-73-73-6 shows calibration to ECCS/Eurocode 3 column curve a. The default values of the elasto-plastic transition parameter yield conservative results for small slenderness ratios. A better agreement is obtained using a = 2.0 for the axial degree of freedom (refer MISOIEP/MPLASMON input).

It is entirely left to the discretion of the user to modify the elasto-plastic transition parameter if ECCS/Eurocode 3 column curve a is to be used. Using the default value a = 0.25 is conservative.

The imperfection level is relatively small, increasing from zero to 0.002.

Figure 3-83-83-7 shows results of calibration to ECCS/Eurocode column curve c using the default value of the a-factor. The agreement is quite good. The imperfection increases from zero to 0.0055.

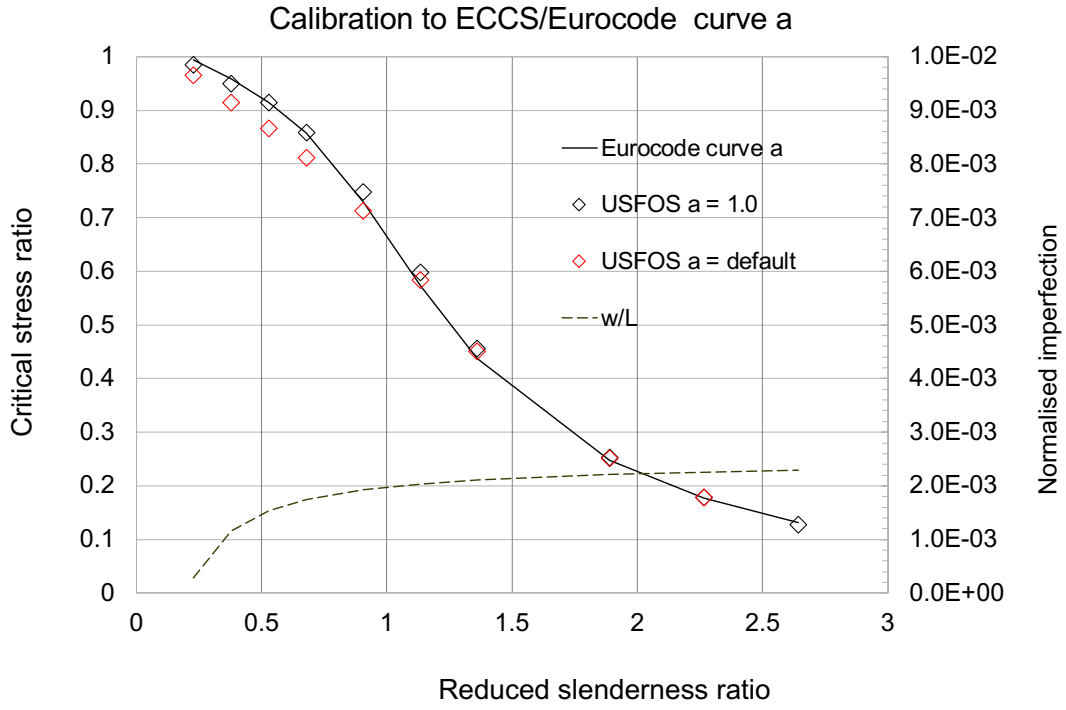

Figure 3-7 Calibration to ECCS/Eurocode 3 – curve a, D/t = 50.

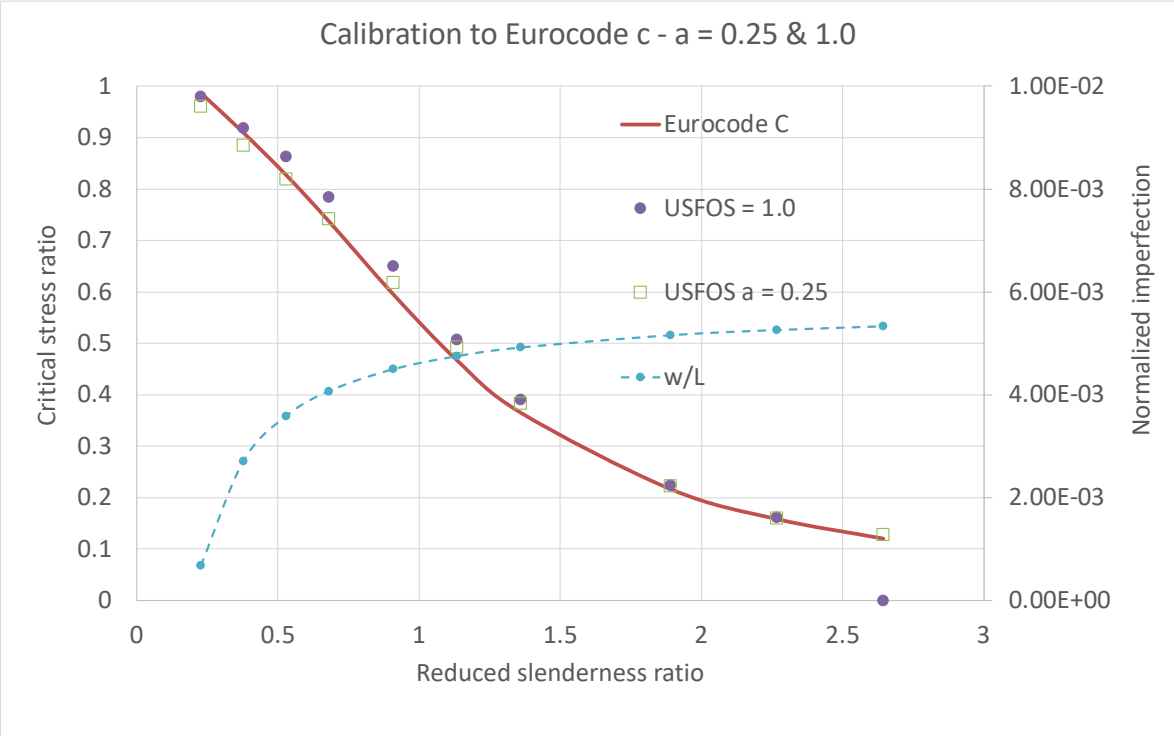

Figure 3-8 Calibration to ECCS/Eurocode 3 – curve c, D/t = 50, a = 0.25 (default) and 1.0

3.5 Eurocode 3 EN 1993-1-2:2005 E -Fire exposed columns

For members subjected to fires the following approach is adopted

$$\frac{A}{W} w_{io} = \mu = \alpha \bar{\lambda}_\theta$$

$$\alpha = 0.65\sqrt{\frac{235}{f_y}}$$

$$\bar{\lambda}_\theta = \bar{\lambda}\sqrt{\frac{k_{f_y\theta}}{k_{E\theta}}} \qquad .3)$$

$$\phi = \frac{1}{2}\left(1 + \alpha\bar{\lambda}_\theta + \bar{\lambda}_\theta^{\,2}\right)$$

$$\frac{f_{cr}}{f_y} = \frac{1}{\phi + \sqrt{\phi^2 - \bar{\lambda}_\theta^{\,2}}}$$

Where $k_{fy\theta}$ and $k_{E\theta}$ are the reduction factors for effective yield strength and elastic modulus, respectively. The square root term is in the range of 1.2 – 1.3, refer Table 1.
The fire reduction curve is very close to curve c, but there is no "break-off" limit $\bar{\lambda}_0 = 0.2$.
This is equivalent to an initial imperfection of

$$\frac{w_i}{l} = 0.0069 \frac{i}{z_0} \qquad .4)$$

When the reduced slenderness at room temperature is reduced

Note *With this formulation the imperfection is independent of the yield strength of the member as opposed to the previous formulation*.

For a thin-walled tube $i / z_0 = 1/\sqrt{2}$ and $\frac{w_i}{l} = 0.0049$. This is approximately 3 times the imperfections used for normal temperatures.

Eurocode 3 specifies that the reduced slenderness ratio shall have a correction because the yield strength and the initial elastic modulus are differently affected by high temperatures. The adjustment factor as a function of temperature is listed in Table 1. The factor varies according to the temperature. At 600^0 C the factor is 1.23%, and thus $\frac{w_i}{l} = 0.006$ for a thin-walled tube. The temperature adjustment factor is automatically taken into account by Usfos when temperature dependent elastic modulus and yield strength are activated.

(In the old formulation the imperfection level depended on the yield strength For a thin-walled tube and yield strength of 250 MPa there was obtained $\frac{w_i}{l} = 0.0038\left(1 - \frac{\bar{\lambda}_o}{\bar{\lambda}}\right)$ and for 355 MPa $\frac{w_i}{l} = 0.0045\left(1 - \frac{\bar{\lambda}_o}{\bar{\lambda}}\right)$, thus somewhat lower values than the new formulation).

Table 1 Adjustment factor for the reduced slenderness ratio for various temperatures

Temperature ^{0}C	$\sqrt{k_{y,\theta} / k_{E,\theta}}$
100	1.00
200	1.06
300	1.12
400	1.20
500	1.14
600	1.23
700	1.33
800	1.11
900	0.94

Fire column curves at various temperatures are plotted Figure 3-93-93-8.

Usfos' calculations of buckling strength are compared with the code curve at 600^0 C in Figure 3-103-103-9. Usfos' results lie slightly above fire curve, but the agreement is satisfactory.

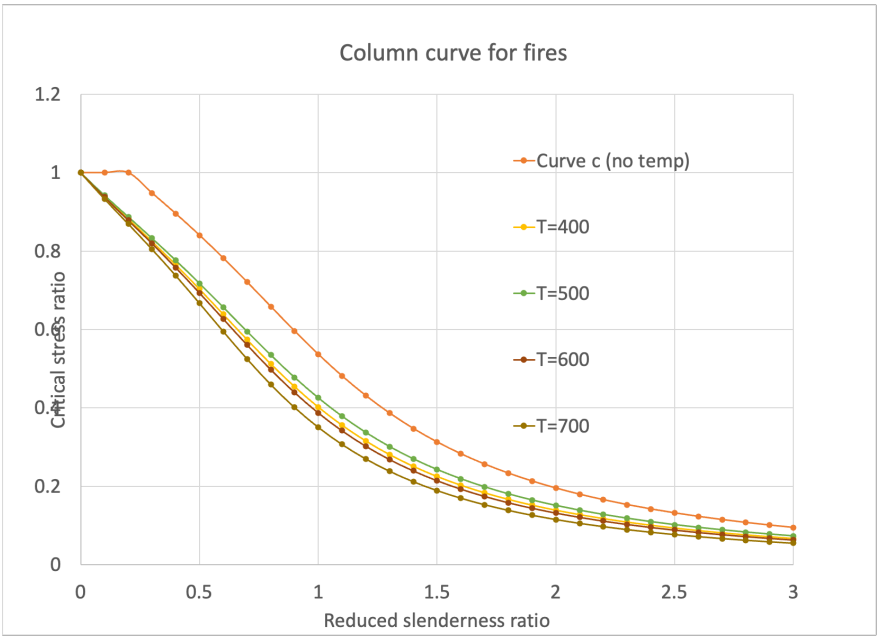

Figure 3-9 Fire column curves for various temperatures. D/t =50

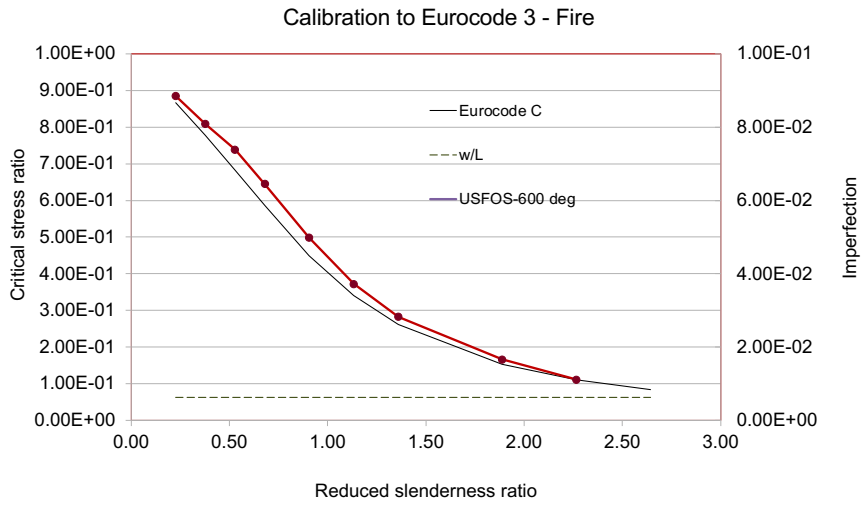

Figure 3-10 Usfos predictions versus Eurocode 3 Fire column curve at 600^0 C, D/t = 50, a = 0.25

4 Considerations of columns/ beam-columns utilization

Columns

The utilisation for a given axial stess $f/f_c < 1$ for a simply supported column will not be linear because of the nonlinearity of the amplification factor. Combining the two

equations in Section1.3 , we get the following expression for the utilization of with respect to initial yielding for an Euler column

$$\frac{f}{f_c}\frac{f_c}{f_{cl}}+\frac{f}{f_c}\frac{f_c A w_0}{W f_{cl}}\frac{1}{1-\frac{f}{f_c}\frac{f_c}{f_E}}=\frac{f}{f_c}\frac{f_c}{f_{cl}}+\frac{f}{f_c}\left(1-\frac{f_c}{f_{cl}}\right)\frac{\left(1-\frac{f_c}{f_E}\right)}{\left(1-\frac{f}{f_c}\frac{f_c}{f_E}\right)}$$

$$=\frac{f}{f_c}-\frac{f}{f_c}\left(1-\frac{f_c}{f_{cl}}\right)\frac{\left(1-\frac{f}{f_c}\right)\frac{f_c}{f_E}}{1-\frac{f}{f_c}\frac{f_c}{f_E}}\le\frac{f}{f_c}$$

Here, f_c is the column buckling value, f_{cl} is the minium of the yield stress and axial local buckling stress, f_E is the Euler buckling stress.

This implies that the utlisation is less than f/f_c for all $f_c/f_{cl}<1$. The deviation depends on the reduced slenderness ratio, which for ISO 19902/NORSOK N-004 is given by

$$\frac{f_c}{f_{cl}}=g\left(\bar{\lambda}\right)=\left(1-0.28\bar{\lambda}^2\right),\quad \bar{\lambda}<1.34$$

$$\frac{f_c}{f_{cl}}=g\left(\bar{\lambda}\right)=\frac{0.9}{\bar{\lambda}^2}\qquad,\quad \bar{\lambda}>1.34$$

and

$$\frac{f_c}{f_E}=\frac{f_c}{f_{cl}}\frac{f_{cl}}{f_E}=g\left(\bar{\lambda}\right)\bar{\lambda}^2=\left(1-0.28\bar{\lambda}^2\right)\bar{\lambda}^2,\quad \bar{\lambda}<1.34$$

$$\frac{f_c}{f_E}=\frac{f_c}{f_{cl}}\frac{f_{cl}}{f_E}=g\left(\bar{\lambda}\right)\bar{\lambda}^2=0.9\qquad,\quad \bar{\lambda}>1.34$$

The utilization with respect to yielding obtained for various levels of axial stress is plotted versus the reduced slenderness ratio, $\bar{\lambda}$, for a simply supported column in **Figure 4-14-14-1.** When λ is small the utilization is equal to f/f_c because the amplification is small and the first term in the Perry Robertson equation predominates. For increasing slenderness ratio, $\bar{\lambda}$, the utilization becomes smaller due to the nonlinearity of the amplification factor and the increased significance of the bending term in the Perry Robertson approach.

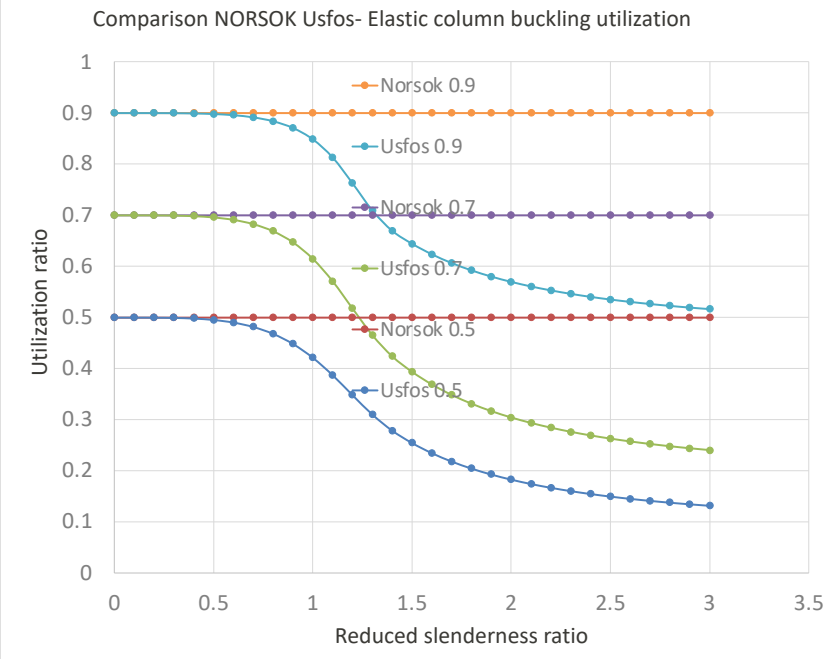

Figure 4-1 Comparison of the utilization for a simply supported column according to ISO 19902/NORSOK N-004 Three different column utilizations are assumed. ISO 19902/NORSOK N-004 utilization is independent of slenderness, while the utilization in USFOS depends on the slenderness ratio $\bar{\lambda}$.

Beam-columns

The utilization of beam-columns in NORSOK is based on a linear interaction between utilization of of a column (with respect to buckling, f/f_c) and the utlilization of a beam in bending

In the beam-column check in ISO 19902/NORSOK a linear interaction between utilization in column buckling and beam bending is assumed

$$\underbrace{\frac{f}{f_c}}_{\substack{\text{column}\\ util.}} + \underbrace{\frac{1}{f_m}\left[\left(\frac{C_{my} f_{my}}{1-\frac{f}{f_{Ey}}}\right)^2 + \left(\frac{C_{mz} f_{mz}}{1-\frac{f}{f_{Ez}}}\right)^2\right]^{0.5}}_{\text{bending utilization}} \le 1.0$$

For simplicity, assume bending in one direction only, thus

$$\frac{f}{f_c}+\frac{1}{f_m}\frac{C_{my}f_{my}}{1-\dfrac{f}{f_{Ey}}}\le 1.0$$

or

$$\frac{f}{f_{cl}}\frac{f_{cl}}{f_c}+\frac{1}{f_m}\frac{C_{my}f_{my}}{1-\dfrac{f}{f_{Ey}}}\le 1.0$$

The nominal bending stresses f_{my} and f_{mz} are reduced by the factors C_{my} *and* C_{mz} (typically < 0.85).

The 2nd order effect is accounted for by a standard expression (magnification factor), which is approximate for deformation patterns not coinciding with the buckling mode. The allowable bending stress, f_m, depends on the diameter/thickness-ratio. As thick-walled members may be allowed to reach the plastic moment capacity, f_m. may artificially exceed the yield stress in linear, elastic analysis

ISO 19902 requires also compliance with the following interaction function

$$1.0-\cos\left(\frac{\pi}{2}\frac{f}{f_{cl}}\right)+\frac{1}{f_m}\sqrt{f_{my}^2+f_{mz}^2}\le 1.0$$

where f_{cl} is the yields stress or the critical stress for local buckling of tube wall.

In NORSOK a linear interaction check is specified (which is stricter)

$$\frac{f}{f_{cl}}+\frac{1}{f_m}\sqrt{f_{my}^2+f_{mz}^2}\le 1.0$$

The reason for cross-sectionlal checks is that the beam column approach may become unconservative for cases with large bending moments and relatively small axial forces due to the C_{my} and C_{mz} reduction factors. This is illustrated in Figure **4-2**24-2 for $C_{my} = C_m =$ 0.85 and in Figure **4-3**34-3 for $C_{my} = C_m = 0.60$, where the utilization of the axial force is normalized with respect to the yield stress or critical stress for local axial buckling . It is observed that the beam-column interaction governs, notably for slender columns. With $C_{my} = C_m = 0.85$ the bending moment must be at least 95% of the allowable bending moment for the capacity equation to become active. With $C_{my} = C_m = 0.60$ it becomes active for relatively stocky columns when the bending moment utilization exceeds approx. 0.5.

It is noticed that the interaction effect decreases with increasing reduced slenderness ratios.

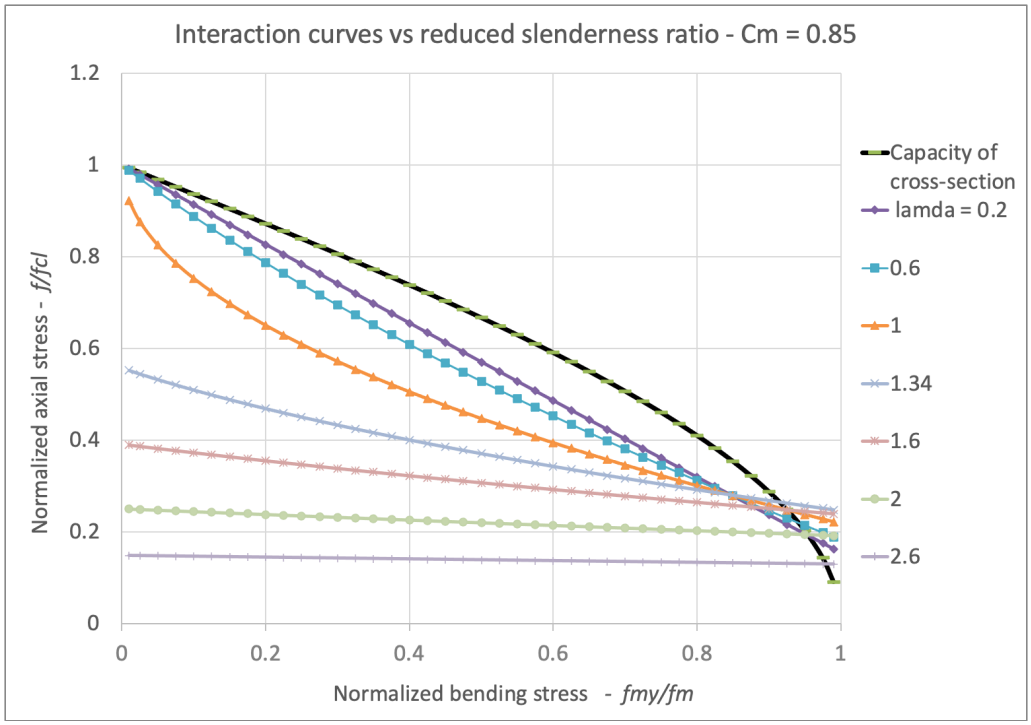

Figure 4-2 Cross-sectional capacity and neam-column interaction for various reduced slenderness ratios according to ISO-19902. C_m -factor = 0.85

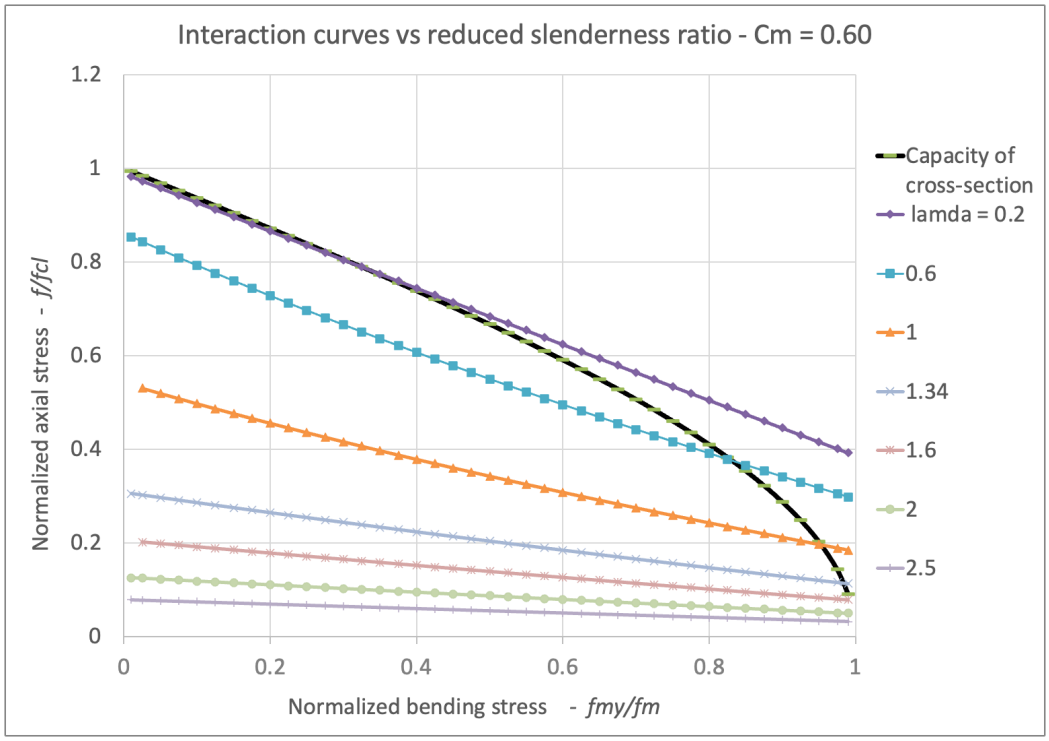

Figure 4-3 Cross-sectional capacity and beam-column interaction for various reduced slenderness ratios according to ISO-19902. C_m -factor = 0.60

The beam-column check in ISO 19902/NORSOK may alternatively formulated as

$$\frac{f}{f_c}+\frac{C_{my}\bar{f}_{my}}{f_m}\le 1.0\,,\quad \bar{f}_{my}=\frac{f_{my}}{1-\dfrac{f}{f_{Ey}}}$$

where $\bar{f}_{my}$ is the bending moment including the 2nd order effect. This interaction is plotted in Figure **4-44** for C_{my} = 0.60 and 0.85.

USFOS does not distinguish between the bending contributions from imperfection and member bending from lateral load and end forces. The 2nd order effect is calculated implicitely in the bending moment. The elastic utilization may be written as

$$\underbrace{\frac{f}{f_y}+\frac{fAe_0}{Wf_y}\frac{1}{1-\dfrac{f}{f_E}}}_{\text{column contribution}=\frac{f}{f_c}}+\underbrace{\frac{M}{Wf_y}}_{\text{beam contribution}}$$

wher e_0 is the imperfection applied to the member during code calibration. The normalized bending stress form the imperfection may also be written

$$\frac{f_{imp}}{f_{cl}}=\frac{fAw_0}{f_{cl}W}\frac{1}{1-\dfrac{f}{f_E}}=\frac{f}{f_c}\left(1-\frac{f_c}{f_{cl}}\right)\frac{\left(1-\dfrac{f_c}{f_E}\right)}{\left(1-\dfrac{f}{f_E}\right)}$$

The capacity of a compact tubular cross-section is governed by the plastic interaction funmction

$$\frac{M}{M_p}-\cos\left(\frac{\pi}{2}\frac{N}{N_p}\right)=0$$

Depending on the diameter/thickness-ratio the pipe may not be compact, so the above formulation may be optimistic. For simplicty, let us assume that M/Mp may be represented by $\bar{f}_{my}/f_m$, which includes the imperfection induced bending f_{imp}/f_{cl}. Let us further assume that $f_{cl}\approx f_m$. This means that we need to reduce the bending moment in the interaction formula to obtain the "true" normalized bending stress

$$\frac{f_{my}}{f_m}=\cos\left(\frac{\pi}{2}\frac{f}{f_c}\right)-\frac{f}{f_c}\left(1-\frac{f_c}{f_{cl}}\right)\frac{\left(1-\dfrac{f_c}{f_E}\right)}{\left(1-\dfrac{f}{f_E}\right)}$$

Normalized axial stress and bending stress that comply with the plastic interaction function are plotted in Figure **4-4**4 for various reduced slenderness ratios. It is observed that the USFOS interaction is cosine shaped but is quite close to the ISO19902 interaction with Cm = 0.6 for relatively stocky columns (reduced slenderness ratios up to approx. 0.7). For slender columns the USFOS interaction lie outside the ISO 19902 curve. The reason for this is two-fold

1) The actual **column** utilization for a certain axial stress, f, is smaller than f/f_c because the amplification is nonlinear and less than proportional with f/f_c. This allows for a larger bending moment, that increases for increasing reduced slenderness ratio.

2) For slender columns the axial stress (compared to the yield stress) is small, so the interaction relationship allows a large bending moment.

Figure 4-4 Interaction diagrams for beam-columns. The ISO 19902 requirement with Cm = 0.60 and 0.85. USFOS interaction diagrams are shown for various reduced slenderness ratios.

The allowable bending moment for $f/f_c = 1$ is just apparent; it converges to zero in USFOS simulations.

The allowable bending stress, f_m, which was assumed equal to the the axial stress for local buckling f_{cl} (often equal to the yield stress) may be larger or smaller depending on cross-section compactness (D/t-ratio).

The beam-column check in ISO 19902/NORSOK N-400 is a practical approach for design of beam-columns, but has as such no direct physical basis. The amplification factors are only exact when the lateral load/end moments create a displacament field that coincireds with the buckling pattern. The reduction factor Cm has no direct phsyical inpterpretation.

USFOS has a more accurate, implicit calculation of the amplification of the bending moment as the axial force increases. Failure of a cross-section results from the evolution of strain internal energy and cross-sectional capacity. There is no need to introduce explicitly amplification factors and moment reduction factors.

The effect of the reduced slenderness ratio is considered to be a true 2nd order effect which can be accounted for in nonlinear finite element simulation. For stocky beam-columns the 2nd order effect is small and the capacity according to USFOS will be close to that of ISO 19902/NORSOK N-400, notably with Cm = 0.6. For slender beam-columns the capacity is larger than ISO 19902/NORSOK N-400. This extra capacity is a real physical effect.

If it should be desired - **conservatively** - to neglect the physical effects decsribed above, USFOS offers the opportunity of **artificially degrading** the interaction curve so that the axial force/bending moment combinations follow the ISO 19902/NORSOK N-004 formulation, see Release Note 9.0.

5 Local effects - “PanCake”

Observations of platform damages after passage of extreme hurricanes in the Gulf of Mexico shown that legs could get a special local buckling mode: the so-called “pancake failure”, see Figure 5-15-15-1

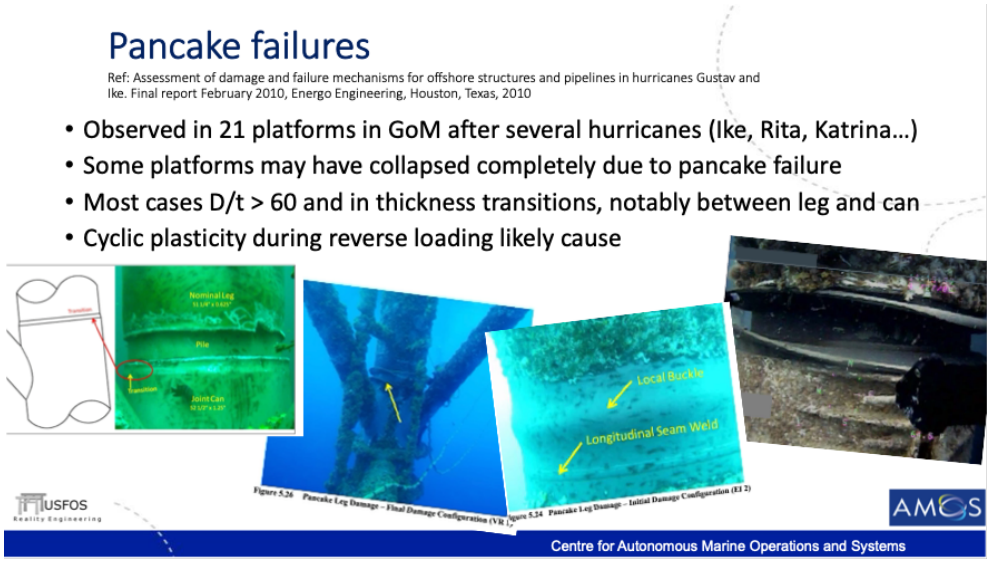

Figure 5-1 – Observed "Pancake" failures in the Gulf of Mexico

Table 5-1 shows that almost all legs had a very high diameter/thickness ratio (in the range of 70-80) and small thickness. The pancake failure took typically place in locations with a significant thickness change in the leg, with a factor of 2 or more. Thickness changes of this order generated significant bending stresses and local deformations in the thin-walled section, which caused local buckling during axial compression. Reversed plasticity during cyclic loading caused complete fracture of the leg in some occasions.

A simple assessment of the elastic stresses and strains induced by the thickness change resulted in an overestimation of the effect. It was therefore decided to estimate the effect from parametric, numerical simulations with the shell element modelling option in USFOS. It was assumed the two legs were flush at the outside. Thus, the thickness change implies an offset that gives rise to axial bending stresses in the shell.

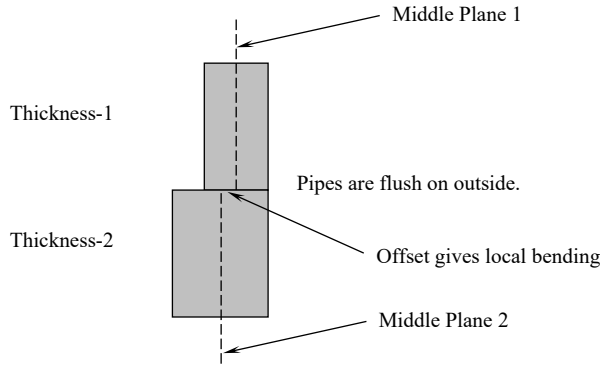

Figure 5-2 Transition to higher wall thickness. Flush outside gives offset.

Table 5-1 Platform with pancake leg damage (Reproduced from Assessment of damage and failure mechanisms for offshore structures and pipelines in hurricanes Gustav and Ike. Final report February 2010, Energo Engineering, Houston, Texas, 2010)

Table 5.5 Platforms With Pancake Leg Damage

Count	Sanized Name	Damage Type	Install Date	Platform Type	Leg Dimensions (at damage)		Leg Joint Can Dimensions		Leg D/t (at Damage)	Leg D/t (at Joint Can)	Elevation of Damage (ft)	Water Depth (ft)	Hurricane	Hmax during Hurricane (ft)	D1 [mm]	T1 [mm]	D2 [mm]	T2 [mm]	T2/T1	
					Diameter (in)	Thickness (in)	Diameter (in)	Thickness (in)												
1	EC 1	Pancake	1988	4-P	"	"	"	"	"	"	67	307	Ike	72.2						
2	EI 1	Pancake	1983	8-P	"	"	"	"	"	"	139	140	Rita	61.6						
3	EI 2	Bulge	1973	4-P	51.5	0.75	53	1.5	"	35	50	153	Ike	62.7	1308	19	1346	38	2.00	Bulge
4	EI 3	Pancake	1976	4-P	39	0.5	39	1.25	78	31	18	153	Ike	N/A	991	13	991	32	2.50	Pancake
5	EI 4	Pancake	1971	4-P	"	"	"	"	"	"	22	172	Lili	N/A						
6	EI 5	Bulge	1973	4-P/4-SK	53	0.625	54	1.625	85	33	88	244	Rita	71.8	1346	16	1372	41	2.60	Bulge
7	EI 6	Pancake	1990	?	"	"	"	"	"	"	"	260	Lili	N/A						Pancake
8	EI 7	Pancake	1971	8-P	51.25	0.625	53.5	1.75	82	31	65	248	Rita	72.6	1302	16	1359	44	2.80	Pancake
9	EI 8	Bulge	1972	8-P	39	0.5	40	1	78	40	76 & 126	246	Ike	72.8	991	13	1016	25	2.00	Bulge
10	EI 9	Pancake	1994	?	33	0.75	33	0.75	44	44	"	414	Ike	78.8	838	19	838	19	1.00	Pancake
11	MC 1	Pancake	1978	8-P/4-SK	"	"	"	"	"	"	35	425	Katrina	71.2						
12	MP 1	Pancake	1997	4-P	"	"	"	"	"	"	6& 58	307	Ivan	76.9						
13	MP 2	Bulge	1977	4-P/4-SK	"	"	"	"	"	"	86	293	Ivan	74.4						
14	SP 1	Bulge	1987	8-P	"	"	"	"	"	"	N/A	340	Ivan	72.4						
15	SP 2	Bulge	1988	8-P	"	"	"	"	"	"	N/A	322	Ivan	72.6						
16	SP 3	Bulge	1998	8-P/8-SK	"	"	"	"	"	"	277	328	Ivan	72.3						
17	SS 1	Pancake & Bulge	1999	4-P	"	"	"	"	"	"	22 & 28	157	Ike	63.2						
18	ST 1	Pancake	1985	4-P	"	"	"	"	"	"	38	56	Rita	42						
19	VR 1	Pancake	1994	4-P	51.25	0.625	52.5	1.25	82	42	46	212	Ike	71.9	1302	16	1334	32	2.00	Pancake
20	VR 2	Pancake	1996	4-P	51.25	0.625	53.5	1.75	82	31	84	300	Rita	75.5	1302	16	1359	44	2.80	Pancake
21	WD 1	Pancake	1970	8-P/8-SK	51.75	0.625	52.25	1.125	82.8	46	320	370	Katrina	75.2	1314	16	1327	29	1.80	Pancake

The analysis model used in the parametric study is shown in Figure 5-35-35-3. In the transition zone, the legs are modelled with shell elements. (As the shell elements are visualized at the middle plane, there is an apparent slope to the thinner element).

At the ends of the shell section ordinary beam elements are connected using the “wheel spoke”-concept.

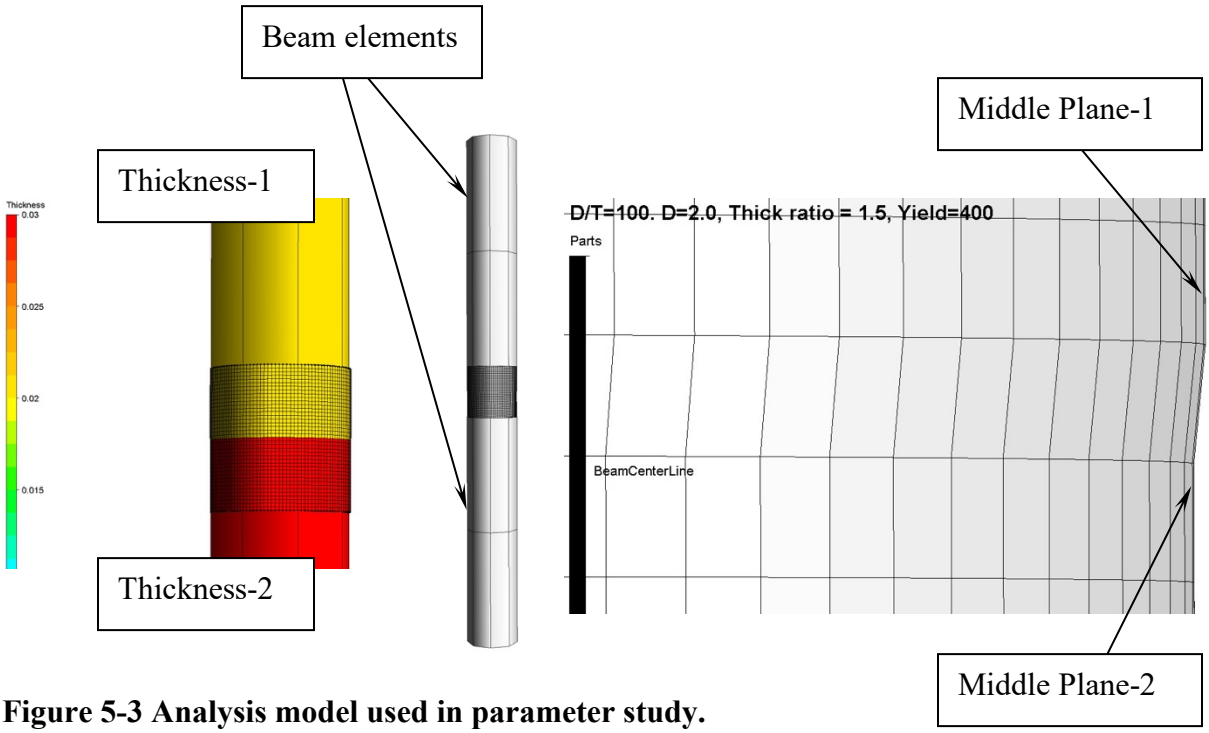

Figure 5-3 Analysis model used in parameter study.

An example of the failure mode obtained in simulation is given in Figure 5-45-45-4 for a transition from 40 mm to 60 mm of a pips with outer diameter 2.0m..

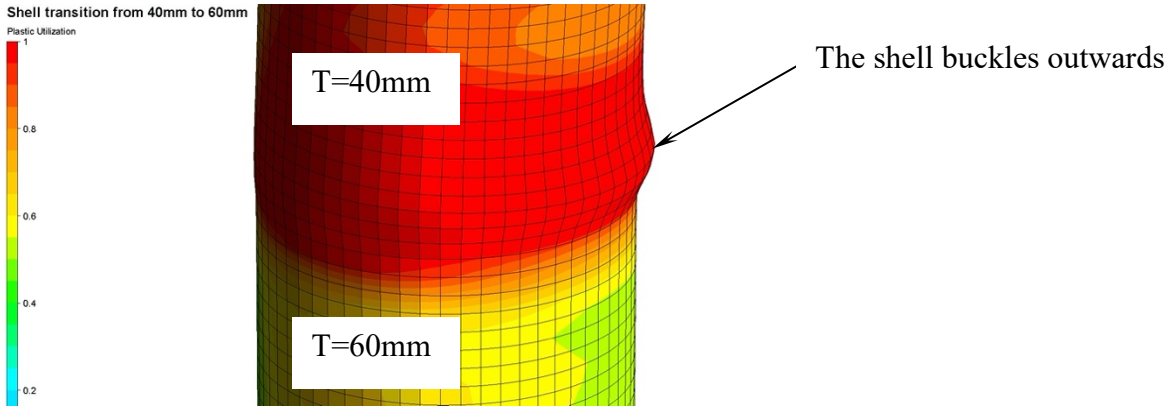

Figure 5-4 - "Pancake" buckling at the transition from 40mm to 60mm

An example of the force-end shortening curve obtained during axial compression is shown in Figure 5-55-55-5. The calibration of the beam element is based on the peak load. Figure 5-65-65-6 how the peak load degrades as the thickness ration increases for different D/t-ratios. The degradation is worse for thin-walled legs, but even for D/t = 30, a reduction is

present. For a given D/t ratio and thickness ratio the actual reduction is estimated by interpolation and extrapolation. The capacity reduction is applied on both the axial force and the bending moment.

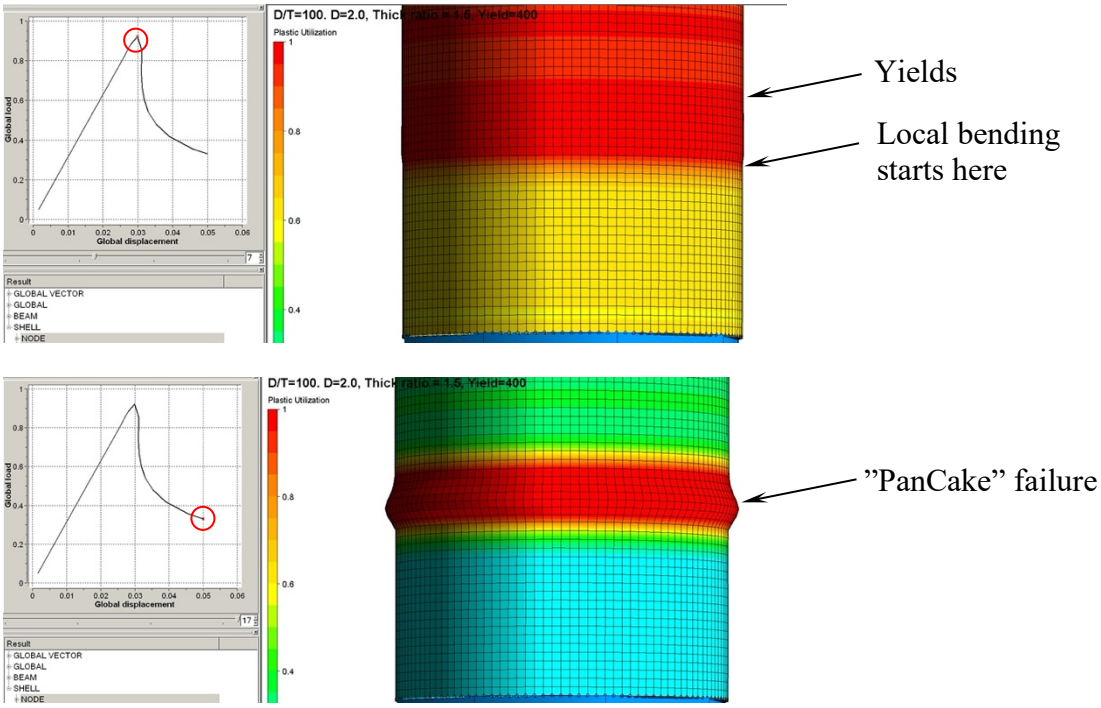

Figure 5-5- "Pancake" buckling at peak load and in the post-collapse range

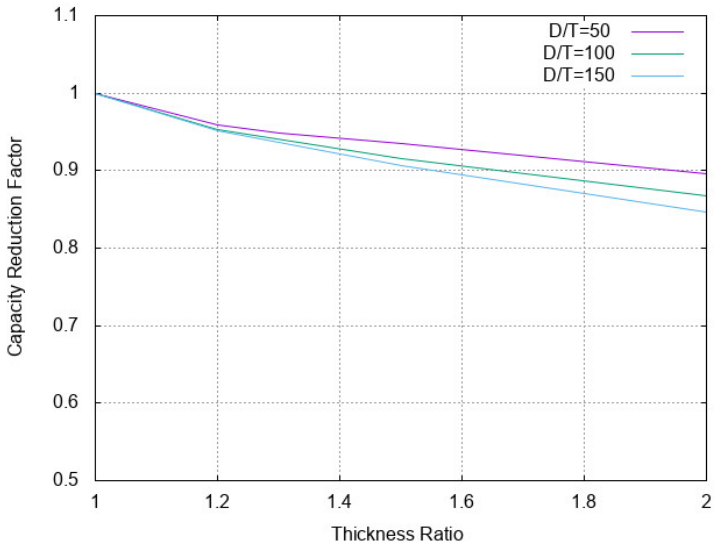

Figure 5-6 Reduction curves for different D/t – and thickness ratios

5.1 Implementation in USFOS

USFOS beam element is extended to account for such "pancake" buckling. It is by default OFF, so the user has to switch ON this option using the following "Switches" command:

```
Switches Solution PanCake ON
```

If the pancake utilization exceeds 1.0, a message is printed to the terminal and to the out file as shown below.

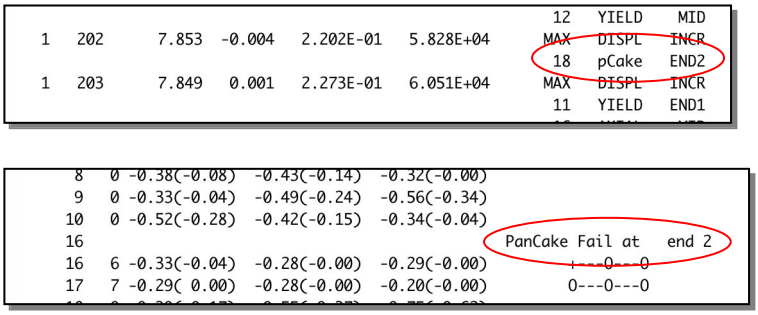

Figure 5-7 - Print to Terminal and to OUT file

When the "PanCake Failure" is detected (pancake utilization > 1), the following happens with the element:

- The cross section capacity degrades.
- The degradation continues each step after the first detected. In practice this means that the element fractures gradually.

Figure 5-85-85-8 shows a simply supported beam, where the left half-part has D/T ratio 50 and the right part has D/T=100.

This means that the thickness ratio between thick and thin pipe is 2.0. A pipe with D/T=100 and a thickness ratio of 2.0 means that the "pan cake" capacity becomes ~87% relative to the perfect case, (with no thickness change).

The degradation takes some steps, and the peak shoots somewhat over the point where the pCake failure was detected. Then the beam starts the unloading (which will continue to ~zero). See also a comparison with and without the PanCake option (Figure 5-135-135-13 on next page).

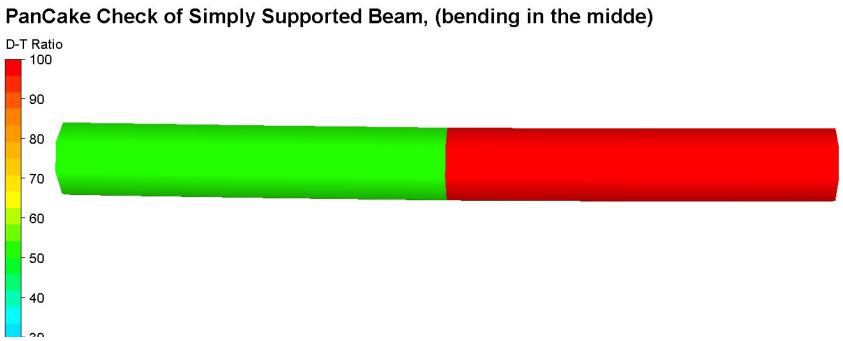

Figure 5-8 - Simply supported beam with load in the middle.

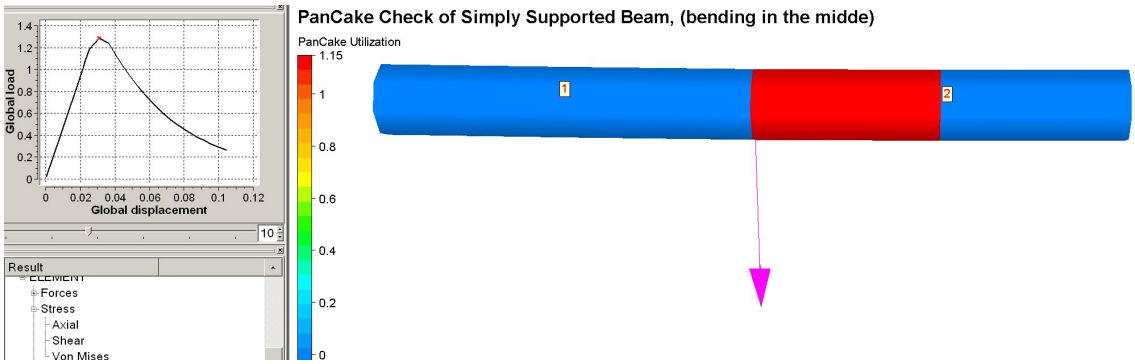

Figure 5-9 – PanCake utilization > 1 for the thin-wall element.

The comparison clearly shows how the conventional model keeps the resistance for increasing displacement. The model with pan cake fails.

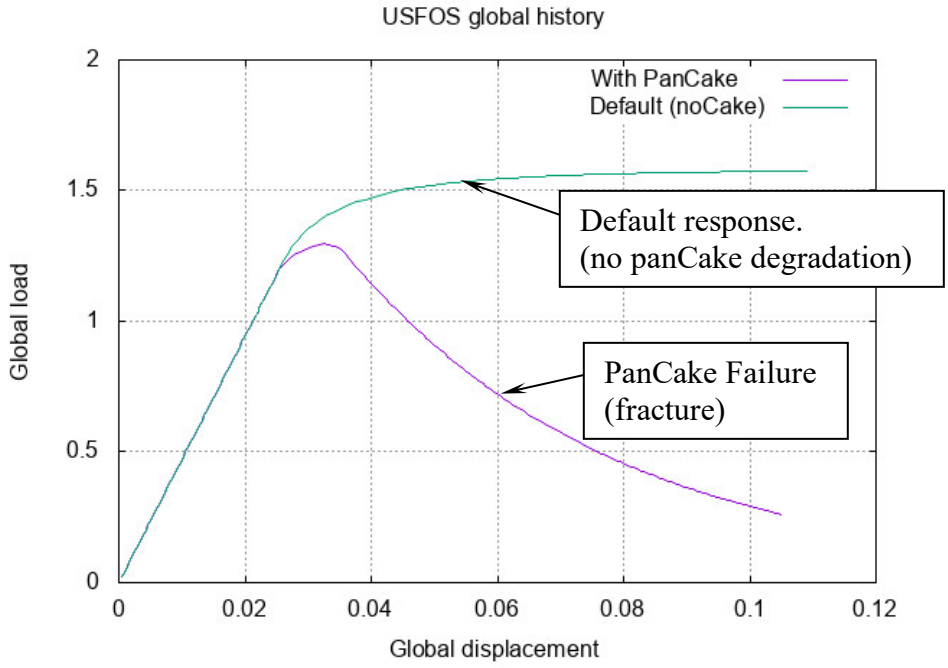

Figure 5-10 - Global Response. Comparison with and without Pan Cake switch.

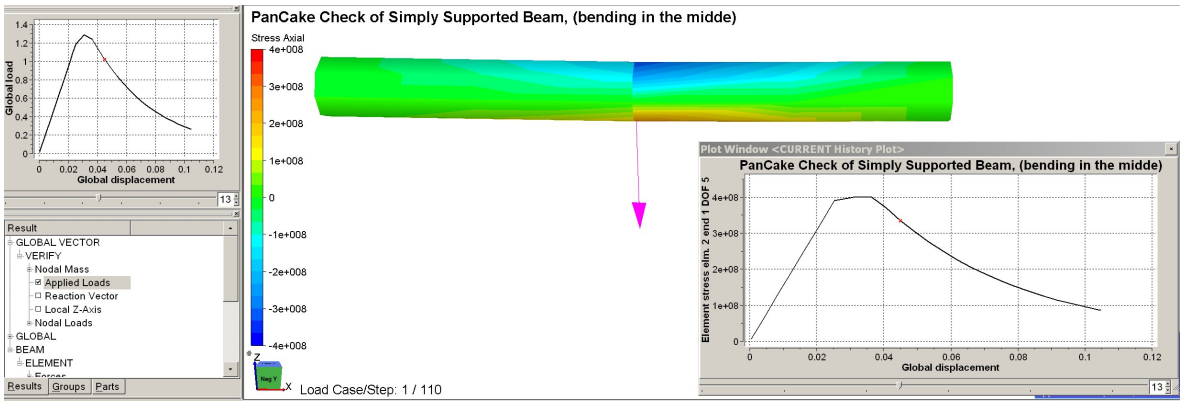

Figure 5-11 - Conventional Beam Bending stress.

Figure 5-125-125-12 shows a 2-D X-braced frame with a horizontal force at the top. The legs have inner piles, which means that the leg to the left gets compression (since the pile has tension). For demonstration purpose, the legs have thickness change in the middle.

In this case, the pancake utilization exceeds 1.0, and this has some impact on the global response, see Figure 5-135-135-13 for comparison Switch = ON/OFF.

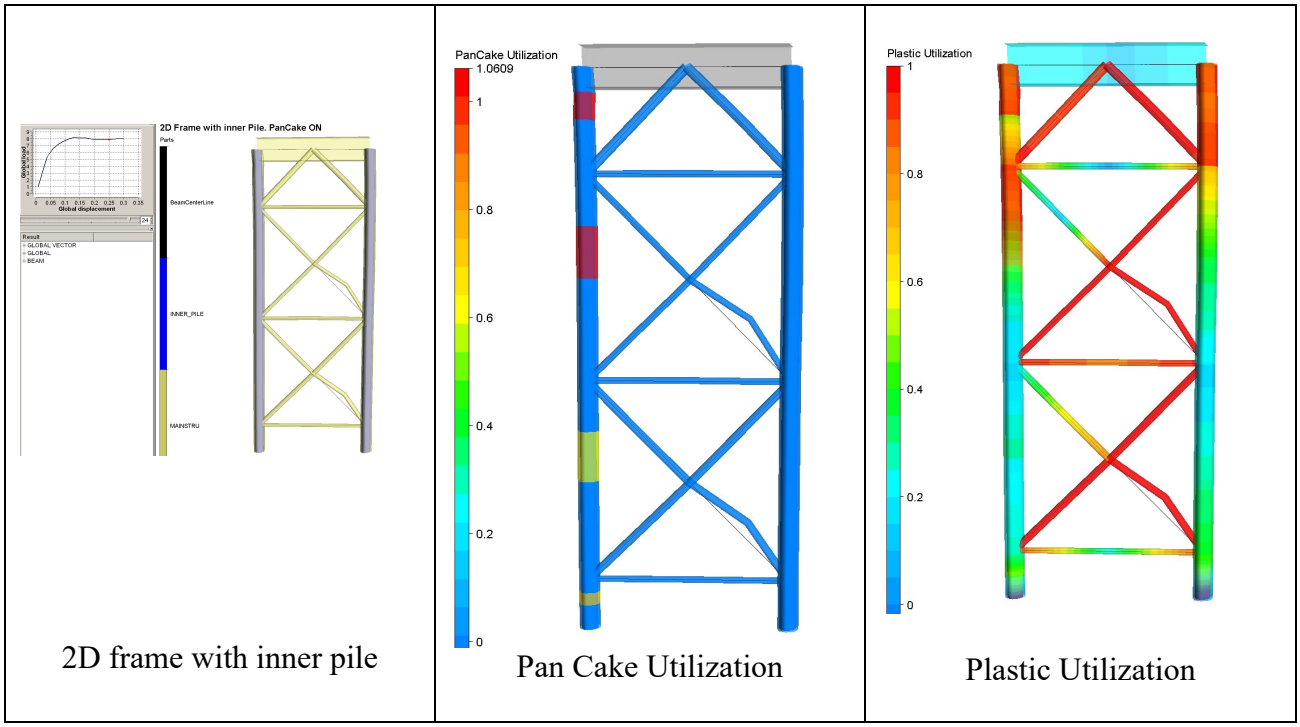

Figure 5-12 - 2D frame with inner piles.

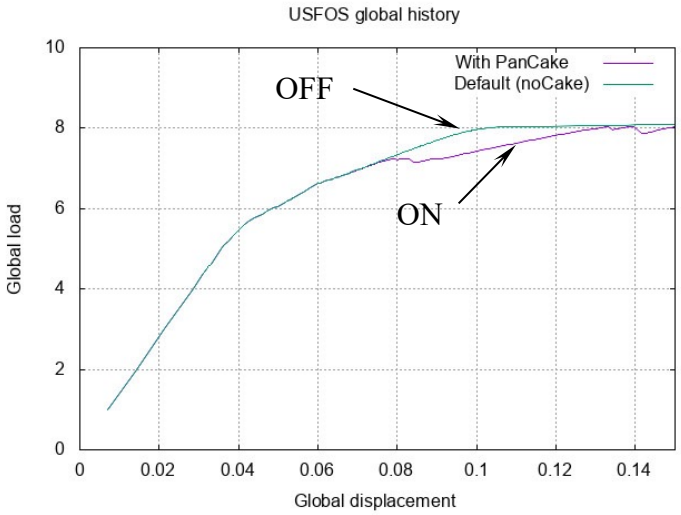

Figure 5-13 - Response with and without pancake option.

6 Dent model for pure bending

The bending-induced dent model assumes that the denting of circular tube is governed by the rotation of a cross-section, such that the total length of the generatrix remains contact. The basic mechanism is illustrated in Figure 6-16-16-1

The present dent growth model is an alternative to the original dent growth model that is governed by the axial force. It is the default and generally preferred model, but it may fail to predict dent growth under bending dominated loading. For a given dent depth the same formulations are used to determine the axial force-bending moment interaction of the cross-section.

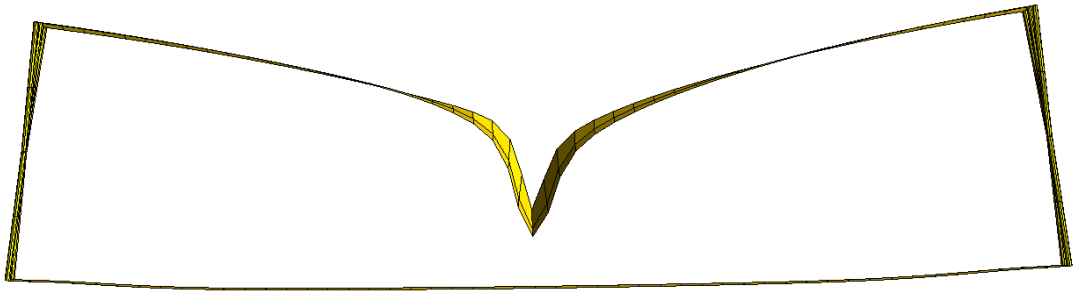

Figure 6-1 Dent depth for rotation of a tubular pipe

The relationship between the dent magnitude and the rotation is empirical and is obtained by numerical simulation of bending of a pipe based on shell finite element modelling. The model is shown in Figure 6-26-26-2. The pipe diameter is 1 m and the length is 4 m. The thickness varies from 5 mm to 40 mm, i.e., from extremely thin-walled section to a compact section. Two different yield stresses have been applied: 300 MPa and 420 MPa. The bending moment is constant over the pipe length. Each end of the pipe is assumed to rotate as a plane section by means of rigid, connecting beam elements.

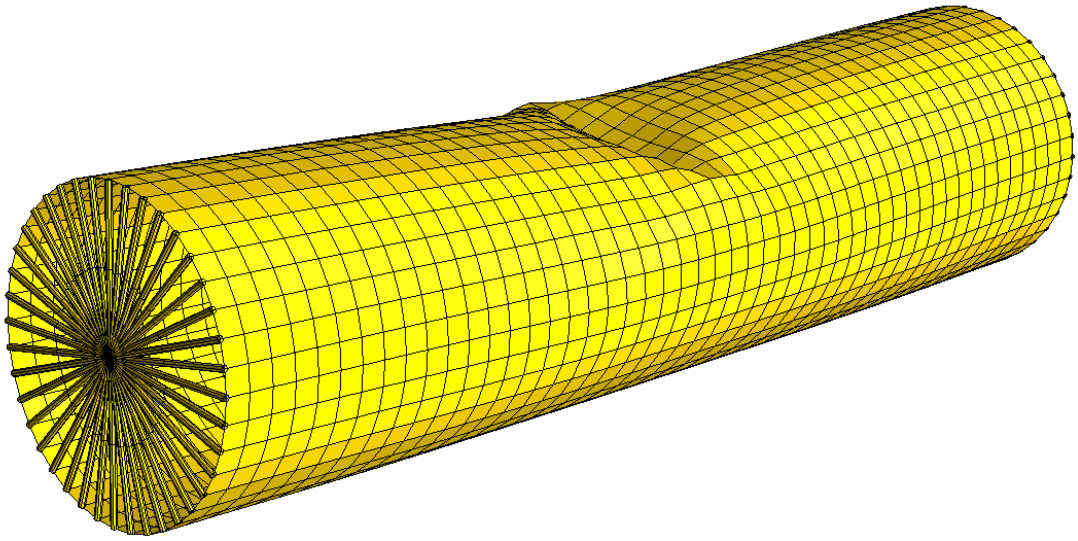

Figure 6-2 Shell finite element model

The pipe undergoes ovalization and local buckling when the moment is increased. The relative dent depth δ/D depth is calculated based on the current distance between the two generatrixes nodes at mid-section shown in Figure 6-36-36-3

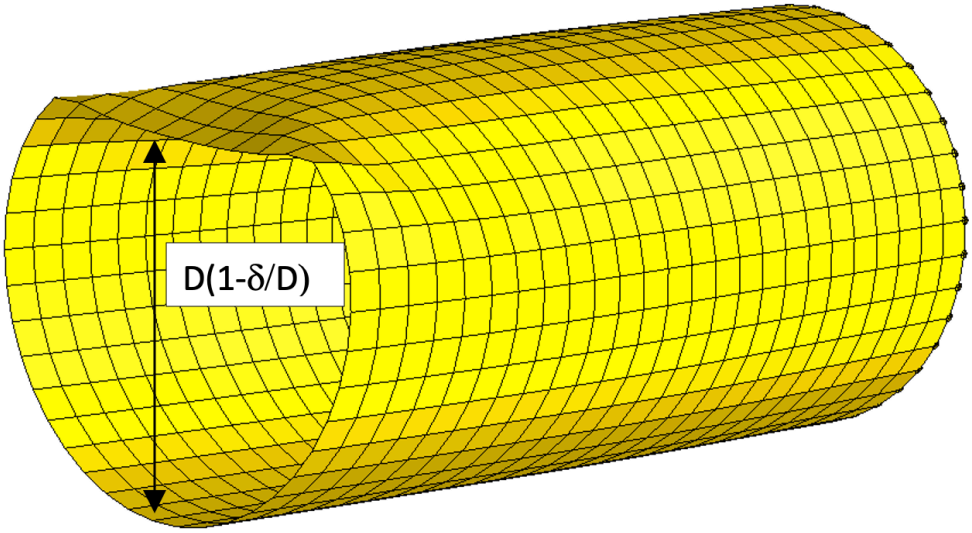

Figure 6-3 Calculation of relative dent depth δ/D

The results of the simulations are given in Figure 6-46-46-4. They show that the dent-depth as a function of the total rotation follows a typical trend. Initially it grows slowly, but at a certain angle it starts to grow rapidly, i.e. local buckling has been triggered. It is observed that local buckling is more evident and occurs for smaller angles when the thickness is small.
The growth of the dent after initiation of local buckling is fairly well described by the following relationship:

$$\frac{\delta}{D} = 1.2\left(\frac{\theta}{2} - \frac{\theta_c}{2}\right)^{0.45} = 0.88(\theta - \theta_c)^{0.45}$$

where θ and θ_c are the total rotation at the hinge and the critical angle for initiation of local buckling.

The critical angle for initiation of local buckling depends on the diameter/thickness ratio and is approximated as:

$$\theta_c = \frac{8}{(D/t)^{1.15}}$$

For $\delta/D < 0.1$, i.e. for angles $0 < \theta < \theta c + 0.008$, a transition curve is used:

$$\frac{\delta}{D} = 0.1\left(\frac{\theta}{\theta_c + 0.008}\right)^2$$

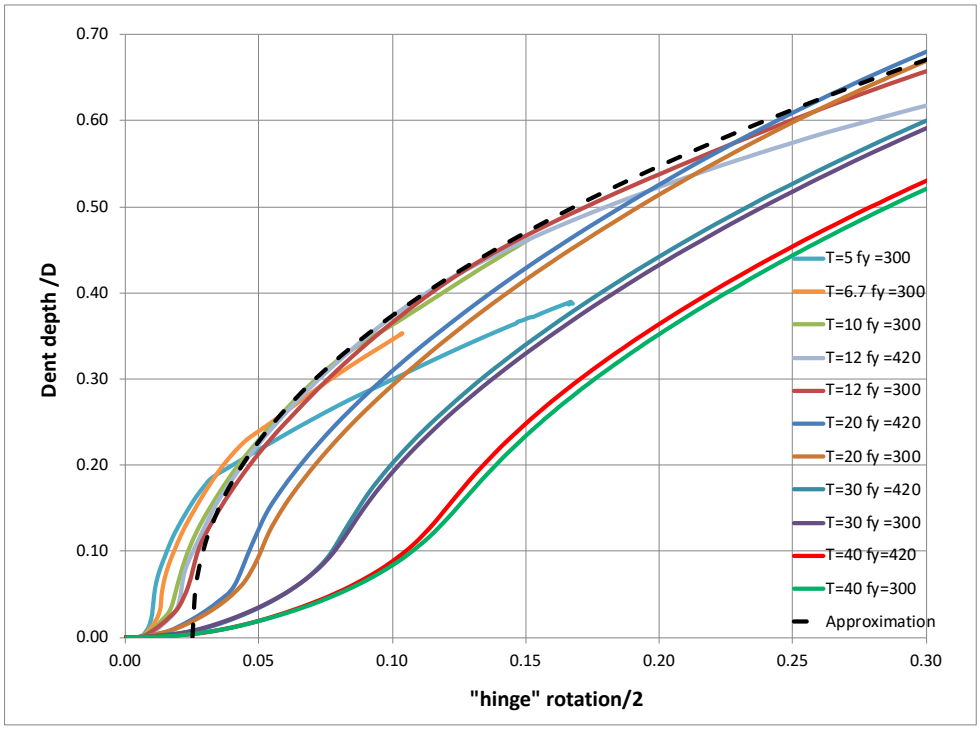

Figure 6-4 Normalized dent depth versus rotation according to shell simulations for a tube with 1.0 m diameter. The diameter thickness ratio varies between 25 and 200(Note: x-axis is $\theta/2$). Approximation is the analytical expression for one example.

6.1 Modification of incremental elasto-plastic stiffness matrix

By means of the consistency criterion for the plastic potential *F*, (*dF=0*), and the normality criterion for the incremental plastic displacement, the incremental elasto-plastic stiffness matrix k_{ep} comes out to be

$$dF = \frac{dF}{d\mathbf{S}}^T d\mathbf{S} + \frac{dF}{d\boldsymbol{\theta}_p} d\boldsymbol{\theta}_p = \frac{dF}{d\mathbf{S}}^T \mathbf{k}_e \left(d\mathbf{v} - d\mathbf{v}_p \right) + \frac{dF}{d\boldsymbol{\theta}_p}^T d\boldsymbol{\theta}_p$$

$$= \frac{dF}{dS}^T \mathbf{k}_e \left(dv - d\lambda \frac{dF}{d\mathbf{S}} \right) + \frac{dF}{d\boldsymbol{\theta}_p}^T d\lambda \frac{dF}{d\mathbf{S}_p} = 0$$

$$\rightarrow$$

$$d\lambda = \left[\frac{dF}{d\mathbf{S}}^T \mathbf{k}_e \frac{dF}{d\mathbf{S}} - \frac{dF}{d\delta} \frac{d\delta}{d\boldsymbol{\theta}_p}^T \frac{dF}{d\mathbf{S}_p} \right]^{-1} \frac{dF}{d\mathbf{S}}^T \mathbf{k}_e d\mathbf{v}$$

$$d\mathbf{S} = \left\{ \mathbf{k}_e - \mathbf{k}_e \frac{dF}{d\mathbf{S}} \left[\frac{dF}{d\mathbf{S}}^T \mathbf{k}_e \frac{dF}{d\mathbf{S}} - \frac{dF}{d\delta} \frac{d\delta}{d\boldsymbol{\theta}_p}^T \frac{dF}{d\mathbf{S}_p} \right]^{-1} \frac{dF}{d\mathbf{S}}^T \mathbf{k}_e \right\} d\mathbf{v} = \mathbf{k}_{ep} d\mathbf{v}$$

where k_e is the incremental elastic stiffness matrix, $dF/d\delta$ is the derivative of the plastic interaction function with respect to the dent size, and $d\delta/d\theta_p$ is the derivative of the dent size with respect to plastic rotation as given above. The last term in the bracket has only two contributions

$$\frac{dF}{d\delta} \frac{d\delta}{d\boldsymbol{\theta}_p}^T \frac{dF}{d\mathbf{S}_p} = \frac{dF}{d\delta} \left[\frac{d\delta}{d\theta_{yp}} \frac{dF}{dM_y} + \frac{d\delta}{d\theta_{zp}} \frac{dF}{dM_z} \right]$$

$dF/d\delta$ is calculated in the same way as the default dent model

6.2 Denting of tubular beam subjected to pure bending

Bending of the circular tube shown in Figure 6-26-26-2 has been simulated with a beam element based on the new dent depth model. Moment rotation relationships for the beam model and the shell models are plotted in Figure 6-56-56-5 for varying D/t -ratios. The shell and the beam model are in reasonable agreement for rotations up to 0.1 -0.15 radians. The moment is somewhat overestimated for compact tubes. For extremely slender tubes the dent growth tends to start somewhat prematurely.

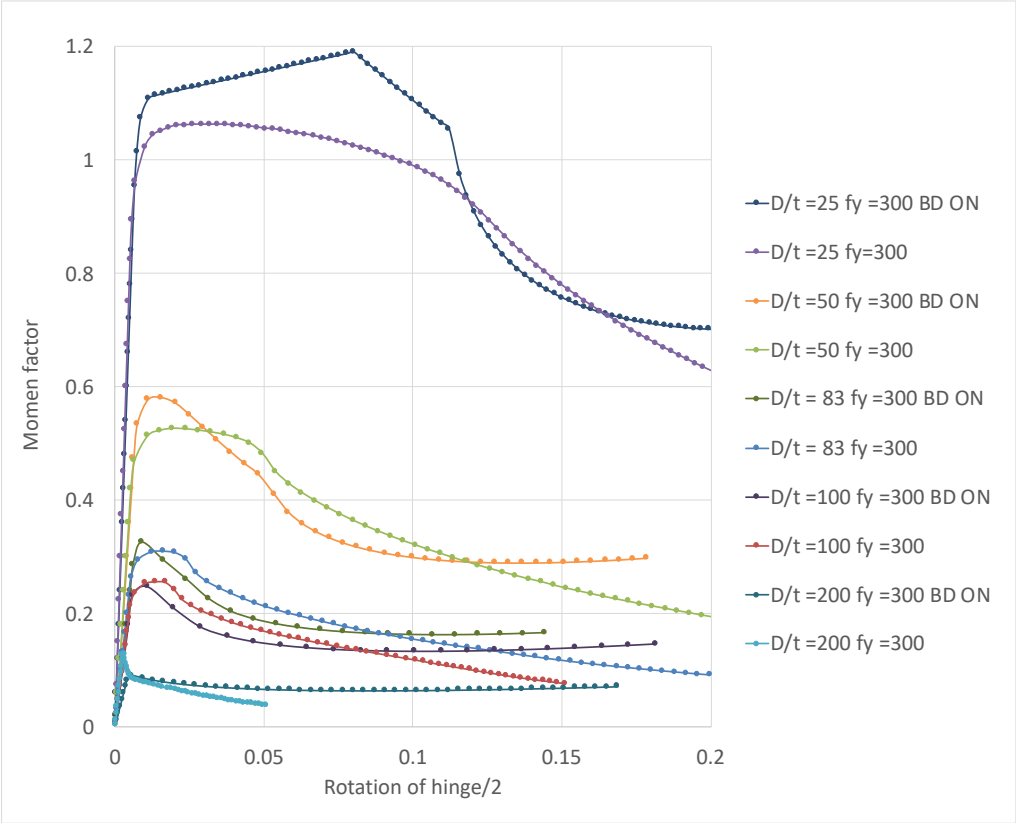

Figure 6-5 Moment-rotation relationship for tubular beams with shell simulations and new model for the beam formulation (Reference moment: 10 MNm.) BendDent ON relations show increasing trend for large rotations

6.3 Comparison of default and new dent model for combined bending and axial compression

The tube model used above is extended with 5 m tubular beams on each side such that the total length is 14 m as illustrated in Figure 6-66-66-6. The beam ends are placed slightly eccentric to the central part (0.063 m) to obtain a bending moment from the axial force. Prior to compression a bending moment is applied and then held constant during increasing axial compression. The initial bending moment amounts to approximately 75%, 50%, 25% and 0% (pure compression) of the plastic bending moment for the pipe. (taken as $2.94 \cdot x\% \cdot \frac{t(mm)}{10}\,[MNm]$). The reference axial load is 18.47 MN.

Axial force-end shortening relationships for two values of section slenderness – D/t = 50 and 100, respectively, are presented un Figure 6-76-76-7through Figure 6-96-96-9. In addition, the simulations with the shell model and the new dent model, results from the original denting model (BD OFF) are plotted.

The agreement between the three models is often good, especially for pure axial loading and moderate bending loads. For D/t = 100 and 75% of the plastic bending moment, the new dent-model underpredicts the axial capacity. It is, however, very unlikely that such slender pipes will be that highly utilized in bending

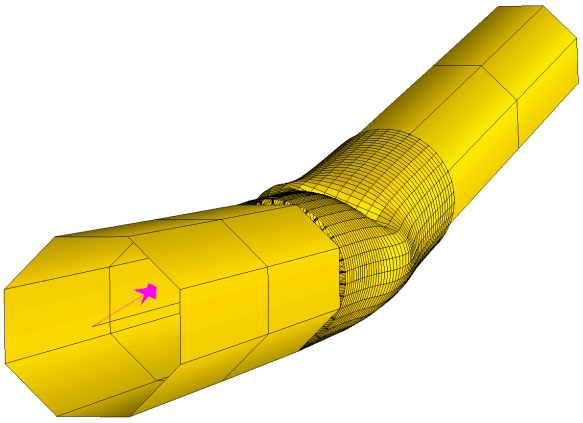

Figure 6-6 Axial compression of column after application of bending moment

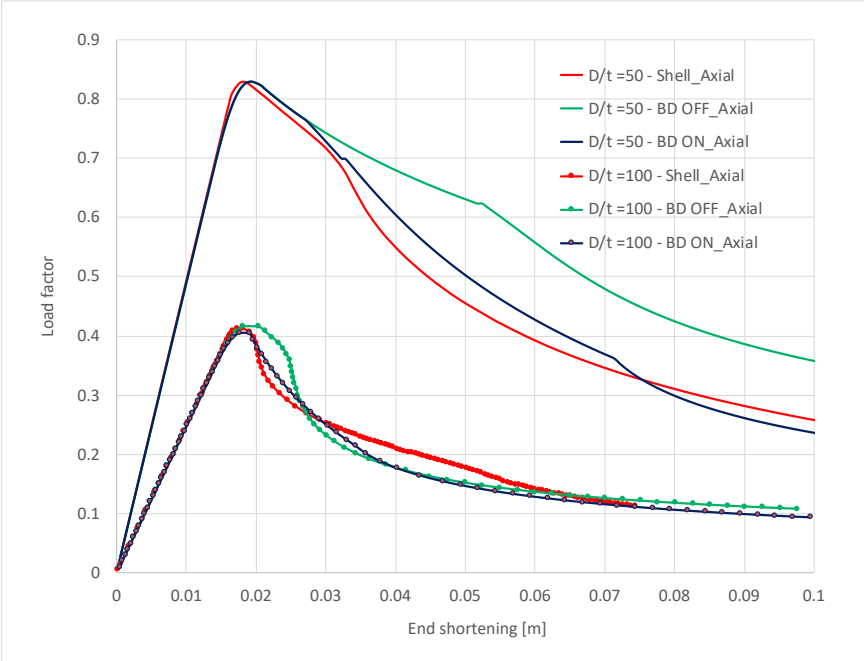

Figure 6-7 Axial force-end shortening relationship for pure compression

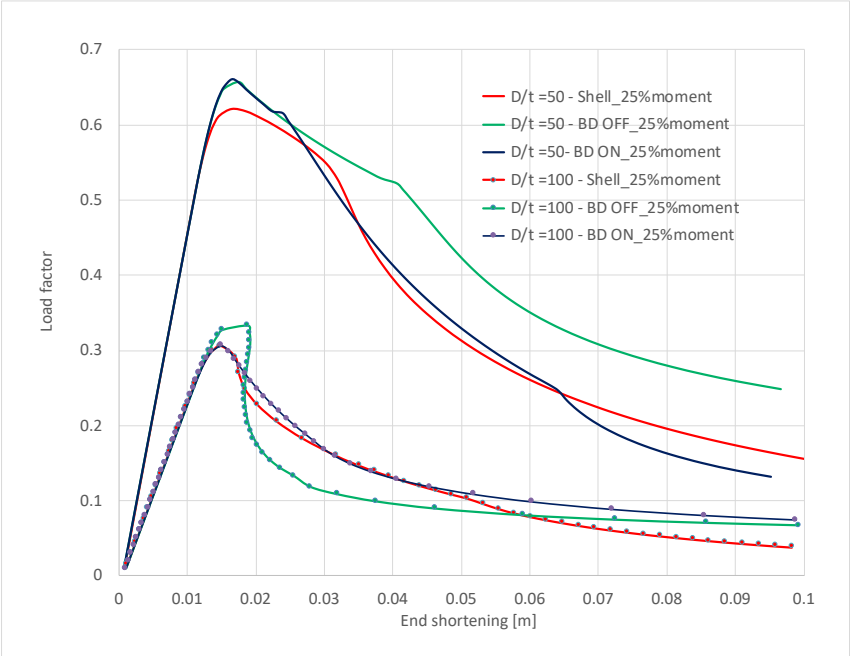

Figure 6-8 Axial force-end shortening relationship 25% bending moment

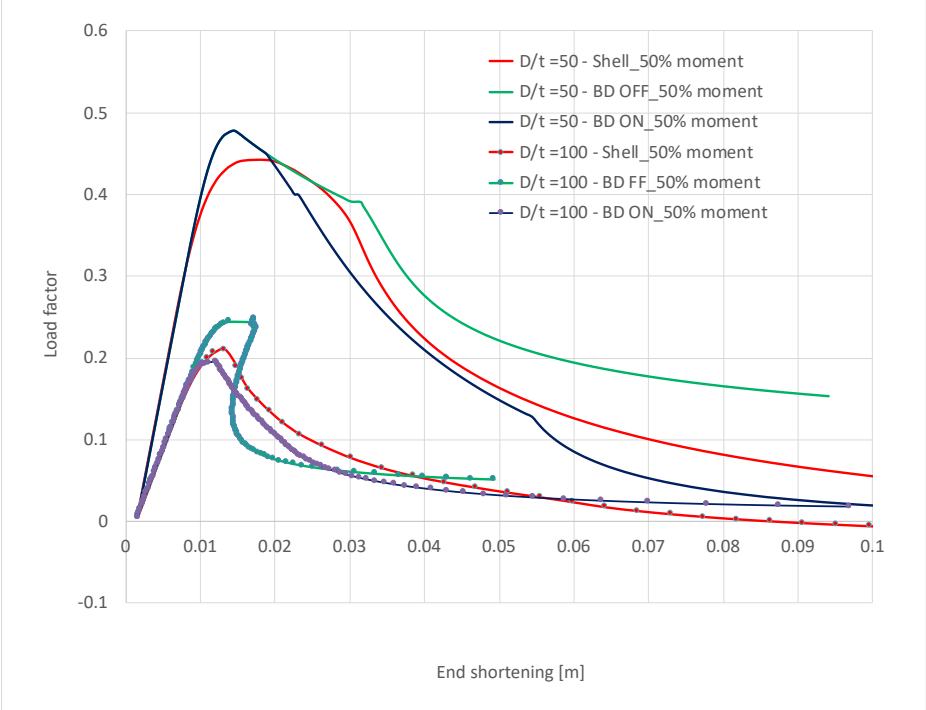

Figure 6-9 Axial force-end shortening relationship 50% bending moment

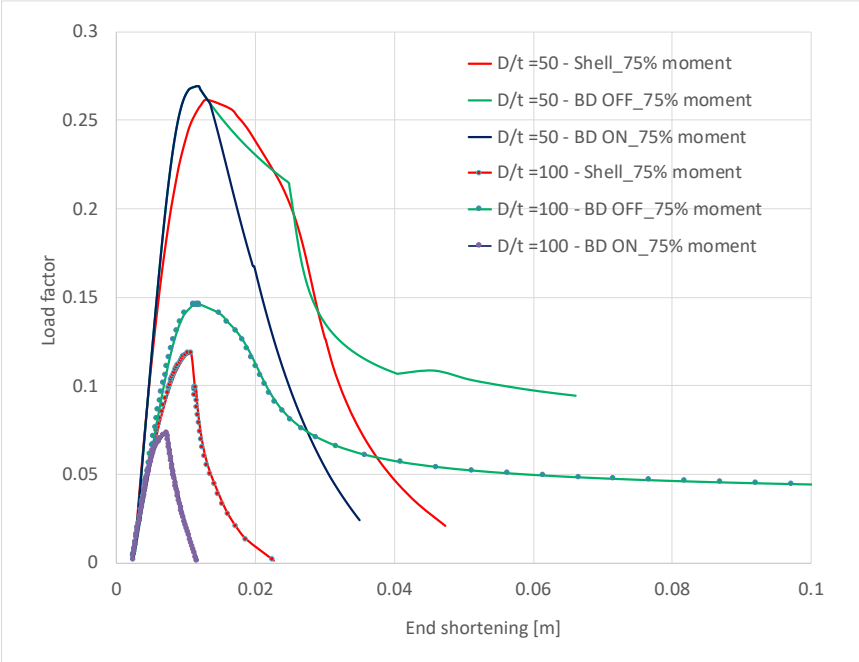

Figure 6-10 Axial force-end shortening relationship 75% bending moment

Finally, results are presented for a relatively compact section with D/t = 33 (t = 30 mm), see Figure 6-116-116-11 and Figure 6-126-126-12. The agreement is good, especially at the peak force. The new dent model seems to work quite well and initiates dent growth earlier than the original model (BD OFF). Due to its compactness, this cross-section can accommodate high bending moments.

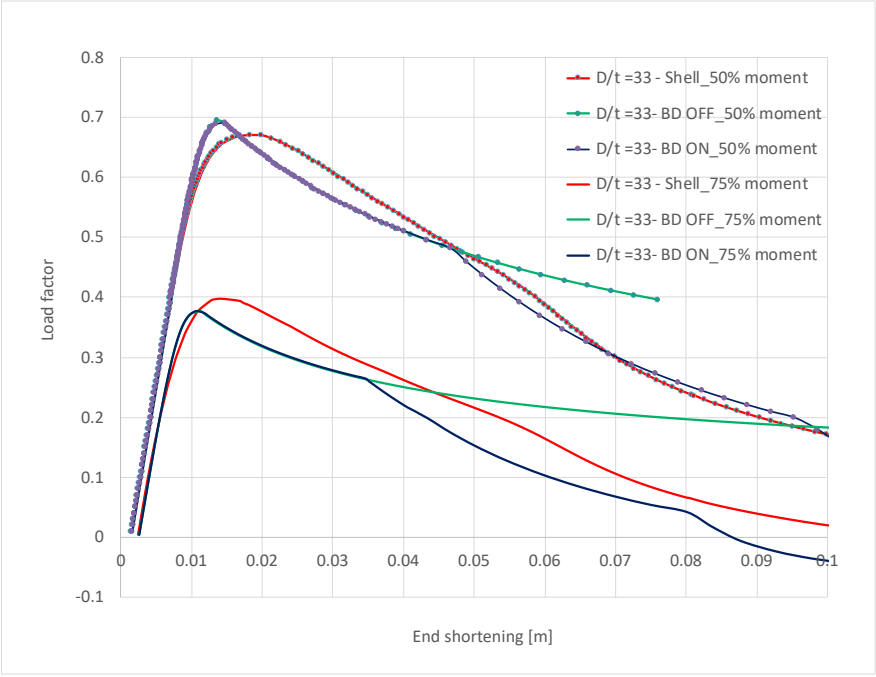

Figure 6-11 Axial force-end shortening relationship D/t =33, 50% and 75 % moment

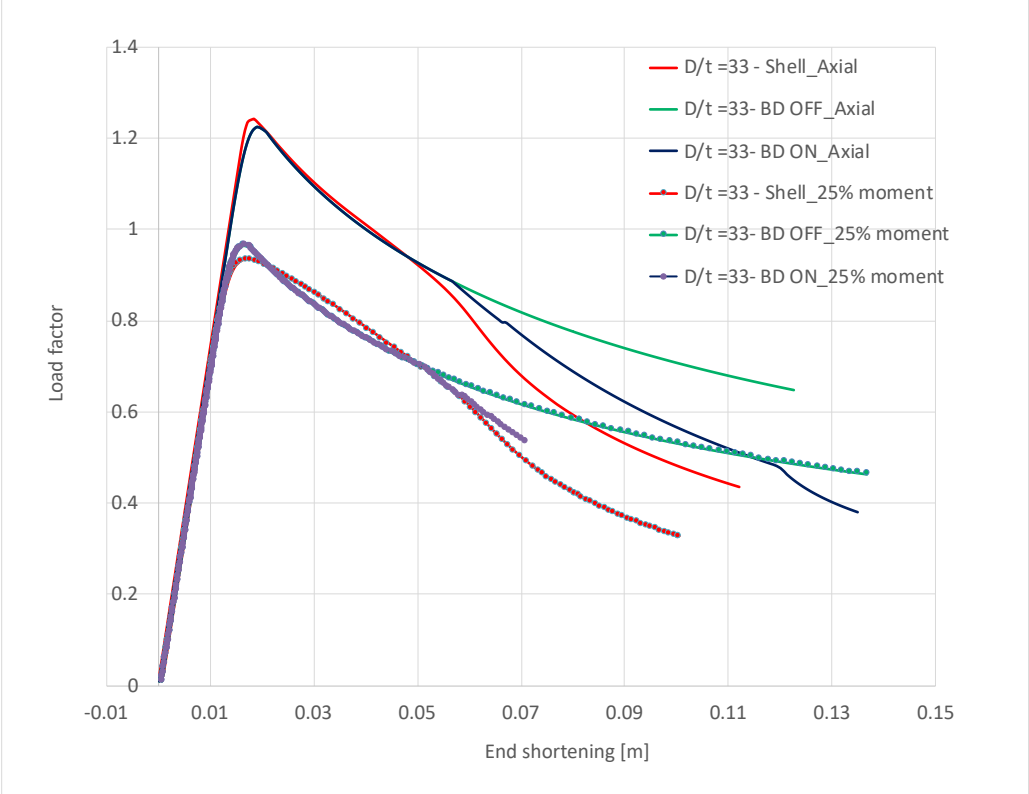

Figure 6-12 Axial force-end shortening relationship D/t =33, 25 % moment and pure axial loading

7 References

API-WSD (R2020) - Recommended practice for planning, designing and constructing fixed offshore platforms - working stress design, API 2nd edition, 2020

API-LRFD (R2019) - Recommended practice for planning, designing and constructing fixed offshore platforms – load and resistance factor design, API 2nd edition, 2019

EUROCODE 3 , PART 1-1 , BS EN 1993-1-1 Design of steel structures – General rules and rules for buildings

ISO 19902:2020(E) Petroleum and natural gas industries. Fixed steel offshore structures

Hellan, Øyvind (1995): Nonlinear Pushover and Cyclic Analyses in Ultimate Limit State Design and Reassessment of Tubular Steel Offshore Structures. (Dr.Ing. Thesis MTA-95-108)

NORSOK STANDARD N-004:2022 Design of Offshore Structures. 2222-06-30

Energo Engineering, Assessment of damage and failure mechanisms for offshore structures and pipelines in hurricanes Gustav and Ike. Final report February 2010, Energo Engineering, Houston, Texas, 2010